JOURNAL OF CHEMICAL INFORMATION AND MODELING

Article

pubs.acs.org/jcim

Computational Studies of Darunavir into HIV-1 Protease and DMPC Bilayer: Necessary Conditions for Effective Binding and the Role of the Flaps

Georgios Leonis,*[,†] Żaneta Czyżnikowska,[‡] Grigorios Megariotis,[†,§] Heribert Reis,[†] and Manthos G. Papadopoulos[†]

[†]Institute of Organic and Pharmaceutical Chemistry, National Hellenic Research Foundation, 48 Vas. Constantinou Avenue, Athens 11635, Greece

[‡]Department of Inorganic Chemistry, Faculty of Pharmacy, Wroclaw Medical University, Szewska 38, PL-50139 Wrocław, Poland

[§]Department of Materials Science and Engineering, School of Chemical Engineering, National Technical University of Athens, 9 Heroon Polytechniou, Zografou Campus, Athens 15780, Greece

Supporting Information

ABSTRACT: Human immunodeficiency virus type 1 protease (HIV-1 PR) is one of the main targets toward AIDS therapy. We have selected the potent drug darunavir and a weak inhibitor (fullerene analog) as HIV-1 PR substrates to compare protease's conformational features upon binding. Molecular dynamics (MD), molecular mechanics Poisson−Boltzmann surface area (MM−PBSA), and quantum-mechanical (QM) calculations indicated the importance of the stability of HIV-1 PR flaps toward effective binding: a weak inhibitor may induce flexibility to the flaps, which convert between closed and semiopen states. A water molecule in the darunavir−HIV-1 PR complex bridged the two flap tips of the protease through hydrogen bonding (HB) interactions in a stable structure, a feature that was not observed for the fullerene−HIV-1 PR complex. Additionally, despite that van der Waals interactions and nonpolar contribution to solvation favored permanent fullerene entrapment into the cavity, these interactions alone were not sufficient for effective binding; enhanced electrostatic interactions as observed in the darunavir-complex were the crucial component of the binding energy. An alternative pathway to the usual way of a ligand to access the cavity was also observed for both compounds. Each ligand entered the binding cavity through an opening between the one flap of the protease and a neighboring loop. This suggested that access to the cavity is not necessarily regulated by flap opening. Darunavir exerts its biological action inside the cell, after crossing the membrane barrier. Thus, we also initiated a study on the interactions between darunavir and the DMPC bilayer to reveal that the drug was accommodated inside the bilayer in conformations that resembled its structure into HIV-1 PR, being stabilized via HBs with the lipids and water molecules.

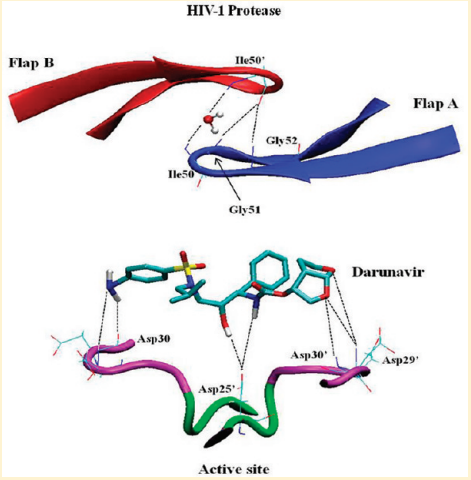

INTRODUCTION

After human immunodeficiency virus type 1 (HIV-1) was recognized as the primary cause of acquired immunodeficiency syndrome (AIDS), the choice of HIV-1 protease (HIV-1 PR) as a target for rational drug design became evident. During viral replication, the aspartic protease HIV-1 PR is produced along with other proteins and essential enzymes. The inactivation of the protease induced after either mutation or chemical inhibition produces noninfectious virus particles with immature morphology, denoting the necessity of HIV-1 PR for viral maturation.[1]

HIV-1 PR belongs to the family of retroviral aspartyl proteases and possesses a symmetric, homodimeric structure. The active site consists of two catalytic triads (Asp25-Thr26-Gly27 in chain A and Asp25′-Thr26′-Gly27′ in chain B) located at the bottom of a large substrate-binding pocket.[2−4] Entrance of a substrate is mainly controlled by the configuration of two glycine-rich β-hairpins (or flaps) that cover the pocket. Numerous experimental and computational studies have investigated conformational changes, principal interactions, and the energetics that accompany HIV-1 PR binding. Specific features such as hydrogen bonding (HB) interactions between an inhibitor and active site residues of the protease,[5−8] the hydrophobic nature of the inhibitor,[9] the way it fits into the cavity,[7] and the presence of water close to catalytic and flap residues[10] are considered necessary for effective binding. Also, several crystal structures of unbound or inhibitor-bound HIV-1 PR have been solved, revealing structural differences of the flaps.[11] Bound forms of HIV-1 PR display a "closed"

Received: January 8, 2012

   dx.doi.org/10.1021/ci300014z | J. Chem. Inf. Model. XXXX, XXX, XXX−XXX

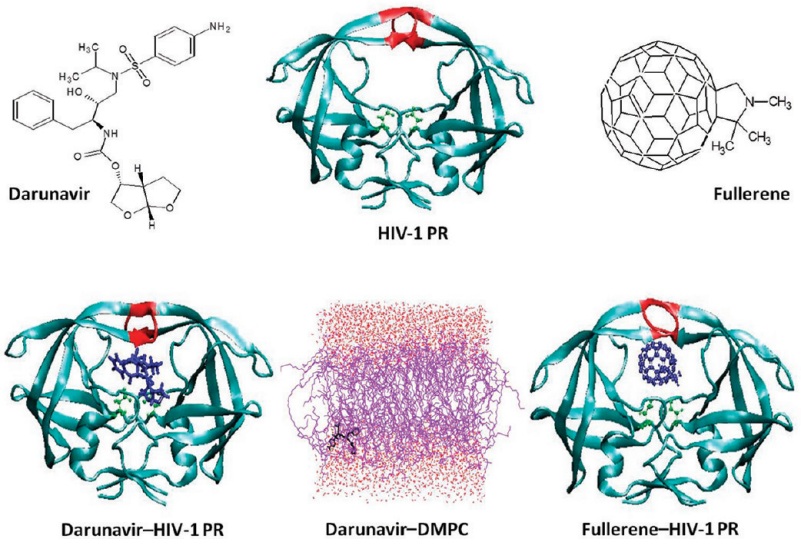

Figure 1. Systems considered in this study: Initial structures for darunavir and fullerene into HIV-1 PR. Each ligand (blue) is found near the [Asp25/Asp25′] active site (green), covered by two glycine-rich flaps (red). A representative conformation of darunavir (black) into DMPC bilayer and the apo form of HIV-1 PR are also shown.

configuration with the flaps oriented toward the bottom of the active site, whereas the structures of the free (apo) protease present an average "semi-open" conformation where the flaps still cover the cavity, yet they are relatively distant from the active site.[11−13] An "open" structure for the apo protease has been reported (PDB ID: 1TW7),[14] and even though it has been shown that such a conformation is stabilized by crystal packing contacts,[15] it still provides a reliable model for ligand access to the binding cavity. A multitude of computational studies considered flap mobility in HIV-1 PR: Hornak et al. reported the permanent closing of the flaps after manual placement of a cyclic urea inhibitor into the HIV-1 PR cavity;[16] the same authors performed long MD simulations for the unbound protease to observe that the flaps open spontaneously before they return to their experimentally observed semiopen form;[3] studies by Toth et al. confirmed similar flap closing upon inhibitor binding, and they also observed comparable results with respect to opening-closing dynamics;[17] finally, McCammon and co-workers used a coarse-grained description for the protease, which was tested on the microsecond time scale:[18] in agreement with the previous observations, multiple opening and closing events occurred, suggesting that the main features of HIV-1 PR dynamics are independent of different simulation approaches.

Most of the previous computational studies were focusing on the dynamics of the protease associated with either a known inhibitor (e.g., a drug) or a suitably designed compound for high potency, both having several polar groups that interact with the active site of the protease. Then, the identification of structural patterns that are associated with effective binding could be obtained; this procedure however may be misleading since some conformational changes would be induced to HIV-1 PR also by a ligand that has minor binding affinity for the protease. Thus, particular structural changes that occur upon binding may not be necessary for *effective* binding. Karplus and co-workers have considered a large and diverse database of HIV-1 PR X-ray complexes to investigate the flexibility of the protein.[19] They concluded that specific structural changes result from the inherent flexibility of the protease, being only slightly affected by the presence of an inhibitor. We are particularly interested in HIV-1 PR behavior, which is solely due to effects induced by effective binding, namely we attempt to "exclude" conformational changes that are ligand-independent. This enables us to identify "intrinsic" characteristics of the bound protease, induced by the mere presence of a ligand regardless its binding effect. Following this rationale, information could be filtered, and conclusions directly related to efficient HIV-1 PR binding may be obtained.

To date, nine HIV-1 protease inhibitors (PIs) have been approved by the FDA to reduce mortality in AIDS patients: saquinavir, ritonavir, indinavir, nelfinavir, lopinavir, atazanavir, (fos)amprenavir, tipranavir, and darunavir.[20] Darunavir is the most recently marketed HIV-1 PR inhibitor (Figure 1). It is a nonpeptidic, highly potent antiviral analog, with a chemical structure designed to increase favorable HB interactions with the backbone of HIV-1 PR in the active site.[6−8,21,22] It exhibits remarkable enzyme inhibitory potency (K_i = 16 pM) and antiviral activity (IC_{90} = 4.1 nM).[9] Ghosh et al. have demonstrated that the enhanced backbone HB interactions are crucial because they cannot be easily altered by mutations since the active site must be conserved to maintain its functionality.[23] Importantly, darunavir is very potent against several drug-resistant mutations with IC_{50} of 3−29 nM for the inhibition of mutants conferring resistance to saquinavir, indinavir, ritonavir, and nelfinavir.[24] MD calculations have been performed to elucidate the binding mode of the darunavir−HIV-1 PR complex, and more accurate quantum mechanical (QM) methodologies have been applied to decompose the energetic impact of binding between binding-cavity residues and darunavir into individual contributions.

Over the past few years, an interest in biological applications involving fullerene derivatives has been developed, mainly due to their size, geometry, free radical affinity, and photophysical properties.[25−27] With the development of functionalized fullerenes the problem of limited aqueous solubility was overcome,[28] leading to the use of fullerenes as agents against viral activity, biological antioxidants, carriers in drug delivery, neuroprotective agents, and photosensitizers, among others.[26] Especially, after the observation that C_{60} fits almost perfectly inside the binding cavity of the protease and the experimental

dx.doi.org/10.1021/ci300014z | J. Chem. Inf. Model. XXXX, XXX, XXX−XXX

confirmation that followed, fullerenes were considered as very promising HIV-1 PR inhibitors.[29] In 1993, Sijbesma et al. were the first to synthesize a fullerene inhibitor of HIV-1 PR;[30] the fullerene was shown to induce strong van der Waals interactions to the surface of the enzyme. Over the years, numerous computational and synthetic approaches have been employed to obtain a variety of fullerene-based HIV-1 PR inhibitors.[26,28] Despite the aforementioned promising features however, the fullerene-based anti-HIV-1 PR drug design is still far from practical value, since fullerene−HIV-1 PR complexes were proven to be poor or moderate PIs. According to our plan mentioned above, we have also chosen a specific fullerene analogue, as a candidate for minimal interactions with HIV-1 PR. This compound has been recently synthesized by Yin et al.,[31] and it meets the requirements of shape, size, and the absence of any polar functional groups (Figure 1). We have performed MD and molecular mechanics Poisson−Boltzmann surface area (MM−PBSA) free energy calculations for the fullerene−HIV-1 PR complex to reveal that the selected compound indeed appeared to have poor inhibitory effect against HIV-1 PR. Therefore, any structural changes induced to HIV-1 PR by both darunavir and the fullerene *may* indicate a "substrate-unrelated", rather inherent behavior of the protease due to the mere presence of a ligand. Thus, structural features that may be expressed independently of specific interactions with a ligand could be considered as not being a necessary and sufficient condition for effective binding. HIV-1 PR and its complexes with darunavir and the fullerene are shown in Figure 1.

HIV-1 PR flaps dynamics is clearly associated with the entrapment of inhibitors. We were motivated to investigate whether there are possible alternative entering pathways or access to the cavity is feasible only via the flap opening. Thus, darunavir has been also placed outside the open flaps of the protease to observe its entering mode. To test the ability of the nonpotent fullerene to enter the cavity, we also performed a similar analysis for its pose outside the flap region (Figure S1).

To complement our study, we have considered the interactions between darunavir and dimyristroyl phosphatidyl choline (DMPC) bilayer in water. It is known that drugs have to cross the water−bilayer regions to exert their biological action inside the cell,[1,32] and according to previous pharmacokinetic studies, darunavir exhibits sufficient membrane permeability that results in intestinal absorption.[33] To the best of our knowledge, a description involving darunavir−lipid bilayer systems is lacking. Thus, we applied MD methodology to test the ability of the drug to penetrate into a bilayer and to identify dominant conformations and physicochemical properties of darunavir in the interior of this structure. A representation of darunavir into DMPC is given in Figure 1.

Our strategy is summarized as follows: initially, MD calculations have been performed for darunavir in aqueous solution; clustering methodology was then applied to rationalize the crystal structure of the drug as a starting conformation for subsequent MD and QM calculations of the darunavir−HIV-1 PR complex in water. Further analysis aimed to explore the binding modes of HIV-1 PR along with the structural changes induced by darunavir. Molecular docking, MD, and MM−PBSA techniques have been used for the fullerene−HIV-1 PR complex in water to estimate the binding affinity of the fullerene for the protease, to decompose the binding energy into individual contributions, and to identify structural patterns associated with fullerene entrapment into HIV-1 PR. A comparison with darunavir−HIV-1 PR would then be obtained. The possibility of an alternative entering pathway to the usual way (through the open space between the flaps) of a ligand to access the binding cavity has been also examined for darunavir and for the fullerene, each being initially placed outside the flaps of the open form of the protease. Finally, an MD simulation has been performed for darunavir outside the DMPC bilayer to monitor the ability of the drug to penetrate the membrane and to study its structural properties and interactions inside the bilayer upon insertion. The apo form of HIV-1 PR has been also considered to distinguish features from the bound protease.

METHODS

Molecular Dynamics of Darunavir and Fullerene in Water. MD simulations have been carried out with the SANDER module from the AMBER 11 simulation package.[34,35] The initial structure for darunavir was taken from the crystal structure of the darunavir−HIV-1 PR complex [Protein Data Bank (PDB) ID code: 2IEN)].[8] Next, the geometry of the drug was optimized with the HF/6-31G** basis set (Gaussian 09),[36] and the general AMBER GAFF force field was used to obtain force field parameters for darunavir.[37] The atomic partial charges were calculated with the ANTECHAMBER module using the RESP method.[38] Comparison with partial charges obtained at the HF/6-31G* level of theory rationalized our approach (Table S1). Solvation in water was achieved using the tLEaP module of AMBER by adding 1575 water molecules (1168 water molecules for the fullerene). Simulations used the TIP3P water model,[39] and each structure was solvated in a truncated octahedral water box to allow for at least 12 Å between each atom of darunavir and the edge of the periodic box. The starting step was the minimization of the system over 5000 steps by keeping darunavir atoms constrained (2500 steps with the steepest descent method and 2500 steps with the conjugate gradient method). The system was allowed to relax further for another 5000 steps by removing the constraints from darunavir. Next, a gentle heating from 0 to 300 K in the NVT ensemble was performed for 200 ps; darunavir was also constrained by a force of 10 kcal mol^{-1} $Å^{-2}$. The same constraints were applied to darunavir during a 200 ps equilibration period at constant pressure; the equilibration was continued for another 200 ps after allowing darunavir and water molecules to move freely. Finally, an unrestrained MD simulation of the system was performed for 200 ns. For the thermalization, equilibration, and MD runs, the SHAKE algorithm[40] was employed for all bond interactions involving hydrogen atoms, thus allowing for a time step of 2 fs. All nonbonded interactions were calculated within a distance cutoff of 10 Å, and a Langevin dynamics temperature scaling[41] with a collision frequency 2.0 ps^{-1} has been used. The same conditions were applied for the simulation of fullerene in water.

Molecular Dynamics of Darunavir−HIV-1 PR, Fullerene−HIV-1 PR, and apo HIV-1 PR in Water. The initial structure for the wild-type (WT) sequence of the closed form of HIV-1 PR was obtained from crystal 2IEN. Protease modifications, including addition of hydrogen atoms, were performed with LEaP in AMBER. Aspartic acid residues of the active site were modeled in their monoprotonated state for both fullerene and darunavir complexes, according to previous experimental and theoretical studies.[42−44] The proteases were represented by the modified AMBER ff99SB force field,[45] while force field parameters and atomic partial charges for the

dx.doi.org/10.1021/ci300014z | J. Chem. Inf. Model. XXXX, XXX, XXX−XXX

fullerene and darunavir were obtained as described above. The explicit solvent treatment was applied to model the effects of solvation. Each structure was solvated using the TIP3P water model, and truncated periodic boundary conditions were applied with a cutoff distance of 10 Å. Crystal water molecules were kept in the structure, while 9505, 8590, and 9510 water molecules were added with LEaP for darunavir−HIV-1 PR, fullerene−HIV-1 PR, and apo HIV-1 PR, respectively. Also, six Cl^- counterions were added to neutralize each system. Long-range electrostatic interactions have been calculated with the Particle Mesh Ewald (PME) method.[46] A four-step energy minimization process with the steepest descent method was used to direct each system toward an energetically favorable conformation. The first step kept the solute (darunavir−HIV-1 PR or fullerene−HIV-1 PR or apo HIV-1 PR) practically fixed with a harmonic force constant of 500 kcal mol^{-1} $Å^{-2}$, while water molecules were allowed to relax. Next, the strength of the restraint was gradually reduced in two steps to 10 kcal mol^{-1} $Å^{-2}$ and eventually to 2 kcal mol^{-1} $Å^{-2}$. Finally, the restraint was removed, to allow all atoms to move freely. Each of the four steps was realized in 5000 cycles with a cutoff of 20 Å. The temperature of the system was then gradually raised from 0 to 300 K under constant volume, over a period of 100 ps. The SHAKE algorithm was applied to constrain all bond lengths involving hydrogen to their equilibrium distance, and a 2 fs time step was used. The Langevin thermostat with a collision frequency of 2.0 ps^{-1} was used to keep the temperature constant. A restraint of 10 kcal mol^{-1} $Å^{-2}$ was also applied to the solute. The same restraint was kept for the next 100 ps of equilibration in the NPT ensemble. A final equilibration stage of 100 ps was performed with all atoms of the system unrestrained. The subsequent MD calculations lasted for 45 ns, for each system. The SHAKE algorithm and Langevin thermostat along with the 10 Å nonbonded cutoff were applied during the heating, equilibration, and production MD periods.

Molecular Dynamics of Darunavir and Fullerene Initially Placed Outside Protease Flaps in Water. Coordinates for the apo and wide open HIV-1 PR (PDB: 1TW7) were obtained after back-mutating the following residues to match the sequence of 2IEN: I10L, N25D, V36M, L46M, V54I, V62I, V71A, A82V, V84I, and M90L. The generalized Born/solvent accessible surface area (GB/SA) implicit solvent model was used to model the effects of solvation[47] for the two poses initiated with darunavir and the fullerene being outside HIV-1 PR. The SHAKE algorithm was also applied for hydrogen-containing bond lengths, and a 2 fs time step was used. The Langevin thermostat (collision frequency 3.0 ps^{-1}) was used for temperature regulation. Both systems were subjected to 2,000 steps of steepest descent minimization; each state obtained from the minimization was next used as the initial conformation for a 50 ps constant-pressure equilibration that brought gradually the systems from 0 to 300 K. Finally, the properly equilibrated conformations were used as the starting point for every subsequent MD simulation. The two complexes were simulated for 45 ns each. A cutoff was not used during the simulations, namely all nonbonded interactions were calculated.

For all trajectories obtained, further analysis [HB, distance and atomic fluctuation calculations, solvent-accessible surface area (SASA), rmsd calculations] was realized with the ptraj module of AMBER. For the HB calculations, a 3.5 Å donor−acceptor distance cutoff with a cutoff of 120° for the donor−hydrogen−acceptor angle were applied.

Molecular Dynamics Simulations of Darunavir in the Water−DMPC Bilayer. Darunavir topology files were produced by PRODGR server.[48] A united atom representation was used for the DMPC molecules, and the topology files were downloaded by the Tieleman Web page (http://people.ucalgary.ca/~tieleman/download.html),[49,50] while water molecules were described by the Simple Point Charge (SPC) model.[51] The bilayer consisted of 128 DMPC molecules in the liquid-crystalline phase and 3655 water molecules. Two different concentrations of darunavir were simulated, namely 1 and 5 molecules, which were all placed initially in the aqueous phase. MD simulations lasted for 240 ns, and all properties have been calculated over the last 60 ns, unless denoted otherwise. Simulations were performed with the GROMACS 4.5.3 MD package.[52−55] Equations of motion were integrated with a 2 fs time step, and all bonds were constrained to their equilibrium length with the LINCS algorithm.[56] The temperature was kept constant at 310 K using the Berendsen thermostat, while the Berendsen barostat was employed for the semi-isotropic pressure coupling of the system at 1 bar.[57] Thus, the Z-direction, which is the normal to the two monolayers is coupled independently to the X−Y plane; in both cases the coupling time constant was set to 1 ps. Long-range electrostatics were treated with PME, while Coulomb and Lennard-Jones interactions have been calculated using a 10 Å cutoff.

Docking Calculations for the Fullerene into HIV-1 PR. Molecular docking calculations were performed with the ArgusLab 4.0.1 program;[58] the fullerene was placed into the binding pocket of the protein close to the active site surrounded by a 25 Å × 25 Å × 25 Å box. During docking the fullerene was considered flexible, while the protease was kept rigid for 10,000 generations with a population size of 50. The crossover rate was set to 0.8 with a mutation rate of 0.2. The convergence criterion was defined at 1.0 kcal mol^{-1}, and the elitism was restricted to five best-atom selection.

Clustering. Clustering calculations for darunavir in water and for darunavir into HIV-1 PR have been performed with a hierarchical approach from the MOIL-View 10.0 program, written by Carlos Simmerling.[59] As the distance metric for the clustering a 3.0 Å rmsd cutoff was introduced to classify 2000 and 2250 conformations of darunavir in water and in HIV-1 PR, respectively. Clustering for darunavir into DMPC has been performed with the UCSF Chimera software.[60] The representative structures produced by the clustering were used for further analysis.

Application of MM−PBSA Methodology To Calculate the Binding Free Energy of the Fullerene Complex. Free-energy calculations consider structural information to estimate binding affinities and their individual contributions.[61,62] Among these approaches, free-energy perturbation (FEP) and thermodynamic integration (TI) techniques, combine statistical mechanics with the thermodynamic cycle to estimate absolute and relative binding free energies in a rigorous formalism.[63−65] Due to their high computational cost however, alternative free-energy methods have been developed over the years to combine optimally the accuracy with computational efficacy: Linear Interaction Energy (LIE)[66,67] is based on a linear approximation of polar and nonpolar free energy terms, and it has been widely used in drug design.[68,69] Several studies have considered LIE and its optimized modifications[70,71] to reach a high level of accuracy with errors between experimental and predicted affinities as low as 1 kcal mol^{-1}.[67] Linear Response Approximation (LRA)[69,72] is another example of such a method

dx.doi.org/10.1021/ci300014z | J. Chem. Inf. Model. XXXX, XXX, XXX−XXX

that accelerates FEP calculations without significantly reducing their accuracy.

A reliable method to estimate the absolute binding free-energy change in protein systems is the molecular mechanics Poisson–Boltzmann surface area (MM–PBSA).[73−75] This method is based on a combination of molecular mechanics (MM) energies for the solute with a continuum solvation model (Poisson–Boltzmann). Normal mode analysis supplements the MM–PBSA method to approximate more accurately the total free energies. In the present work, we have employed MM–PBSA to test the inhibitory potency of the fullerene against HIV-1 PR. For the fullerene–HIV-1 PR complex, the change in the binding free energy (ΔG_{bind}) drives the binding process

$$\text{HIV-1 PR} + \text{Fullerene} \rightarrow \text{Complex}$$

Initially, 4500 MD snapshots (equally spaced at 10 ps intervals) of the complex (stripped of water molecules and counterions) were considered. This spacing would be sufficiently far apart in order to obtain structures that are uncorrelated, yet an adequate population of structures is obtained to ensure a relatively low statistical error.[76] Based on the assumption that conformational changes are not significant upon binding, all snapshots were obtained from the trajectory of the complex (instead of running three independent simulations for HIV-1 PR, inhibitor, and complex), according to the "single trajectory approach".[75] For each snapshot a free energy for the complex, fullerene, and HIV-1 PR is calculated, and the total binding free energy ΔG_{bind} is computed using the following general equation

$$\Delta G_{bind} = G_{complex} - (G_{HIV\text{-}1\ PR} + G_{fullerene}) \quad (1)$$

$G_{complex}$, $G_{HIV\text{-}1\ PR}$, and $G_{fullerene}$ are the energies for the complex, the receptor, and the inhibitor, respectively. The binding energy can be expressed as a combination of enthalpic and entropic contributions

$$\Delta G_{bind} = \Delta H - T\Delta S \quad (2)$$

The enthalpic term in eq 2 is calculated as

$$\Delta H = \Delta E_{MM} + \Delta G_{solv} \quad (3)$$

where ΔE_{MM} defines the molecular mechanical (MM) free-energy change upon complex formation in the gas phase, and ΔG_{solv} is the solvation free energy. ΔE_{MM} is further divided into Coulomb interactions and van der Waals interaction terms

$$\Delta E_{MM} = \Delta E_{ele} + \Delta E_{vdW} \quad (4)$$

For these nonbonded terms no cutoff was applied. Furthermore, the solvation term of eq 3 is defined as a sum of polar (ΔG_{PB}) and nonpolar (ΔG_{NP}) contributions

$$\Delta G_{solv} = \Delta G_{PB} + \Delta G_{NP} \quad (5)$$

The polar term of the energy was calculated by solving the Poisson–Boltzmann equation (PB method)[77] using the PBSA module of the AMBER suite, and the nonpolar contribution to the solvation free energy was determined as a function of SASA[78]

$$\Delta G_{NP} = \gamma \text{SASA} + \beta \quad (6)$$

In the above equation, the standard values for surface tension γ = 0.00542 kcal mol^{-1} Å^{-2} and for offset β = 0.92 kcal mol^{-1} were used. A probe radius of 1.4 Å was considered. The dielectric constant for the solute was 1.0, and the solvent dielectric constant was 80.0. ΔG_{NP} was computed via eq 6, with the linear combinations of pairwise overlaps (LCPO) method.[79] Finally, the entropic term $-T\Delta S$ (eq 2) was calculated by normal-mode analysis using the NMODE module of AMBER, over only 450 equally spaced snapshots to save computational time.

The validity of free-energy decomposition into individual contributions by the MM–PBSA method could be verified in the more rigorous Free-Energy Perturbation (FEP) formalism: Bren et al. performed FEP calculations to test the reliability of the free energy decomposition by estimating the solvation free energy of magnesium complexes of deoxyribonucleoside triphosphates in water.[80] It was observed that the decomposition was associated with an inherent (nonadditivity) error that could be decreased by increasing the number of perturbation steps. Thus, when 51 (or more) FEP steps were used, a nonadditivity error <0.02 kcal mol^{-1} was obtained for the solvation free energies. Therefore, each system could be satisfactorily described by the sum of its constituents, in a few perturbation steps. In a related study, the free energy decomposition is described in a rigorous formulation that employs a probability theory tool, namely Thiele cumulants.[81] It was shown that the accuracy of the free energy decomposition is decreased due to mixed potential energy terms in Thiele cumulants of second and higher orders.

Solvent-Accessible Surface Area Calculations. SASA calculations were based on the rolling ball algorithm described by Shrake and Rupley.[82] A value of 1.4 Å was used as a probe radius for the water molecule. SASA values were obtained for all systems inside the binding cavity of the protease as well as for the solvated fullerene and darunavir.

Darunavir–HIV-1 PR Intermolecular Interaction Energy Partitioning. To unravel in more detail the origin of stabilization of the darunavir–HIV-1 PR complex, we performed the intermolecular interaction energy partitioning using the variational–perturbational scheme[83−88] implemented in a modified version of the GAMESS US package.[89,90]

In this approach, the total intermolecular interaction energy calculated at the Hartree–Fock level of theory (ΔE^{HF}) is decomposed into the first-order electrostatic ($\varepsilon^{(10)}_{el}$), Heitler-London exchange (ε^{HL}_{ex}), and delocalization components ΔE^{HF}_{del}

$$\Delta E^{HF} = \varepsilon_{el}^{(10)} + \varepsilon_{ex}^{HL} + \Delta E_{del}^{HF} \quad (7)$$

The electrostatic energy represents the Coulomb interaction of the monomers' charge distributions, while ε^{HL}_{ex} contains the main exchange contribution to the interaction energy computed as the difference $\Delta E^{HL} - \varepsilon^{(10)}_{el}$. The sum of the first two terms on rhs of eq 7 is the Heitler-London interaction energy (ΔE^{HL}), and it is obtained as an antisymmetrized Hartree product of monomer wave functions. The delocalization term (deformation component) contains charge transfer and polarization effects. The variational-perturbational interaction energy decomposition scheme has been successfully employed in studies on the nature of interactions in plethora of systems, including nucleic acid base complexes,[91,92] amino acids,[93] molecular crystals,[86] or shellvented ions.[94] Since the dimer-centered basis set is employed during the calculations, the total intermolecular interaction energy and its components were free from the basis set superposition error.

The representative structure of darunavir–HIV-1 PR after performing clustering in the complex has been considered, while several residues of the protein were removed to make

dx.doi.org/10.1021/ci300014z | J. Chem. Inf. Model. XXXX, XXX, XXX–XXX

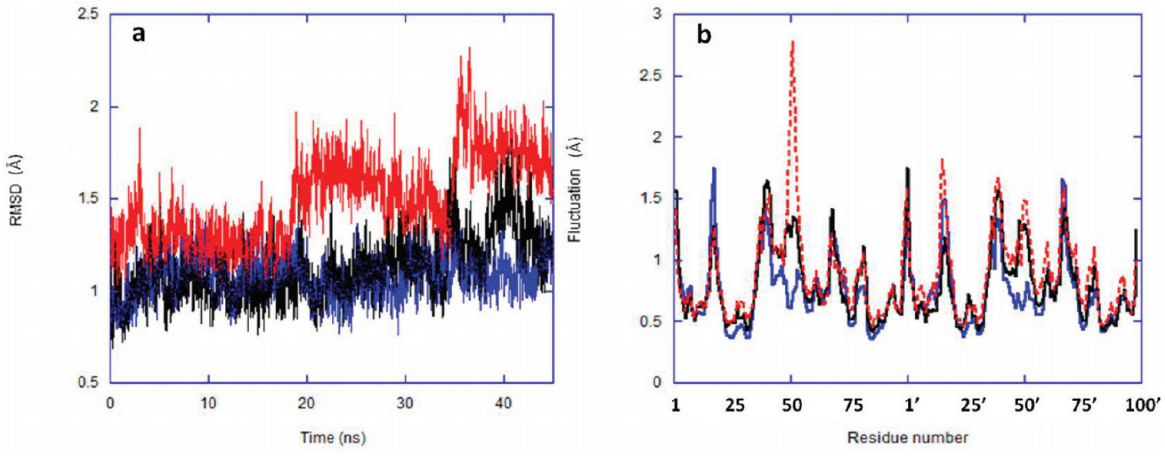

Figure 2. (a) rmsd and (b) Cα atomic fluctuations of HIV-1 PR in its darunavir-bound (blue), fullerene-bound (red), and apo (black) forms. For the rmsd calculations all HIV-1 PR forms were overlapped on the crystal structure of 2IEN.

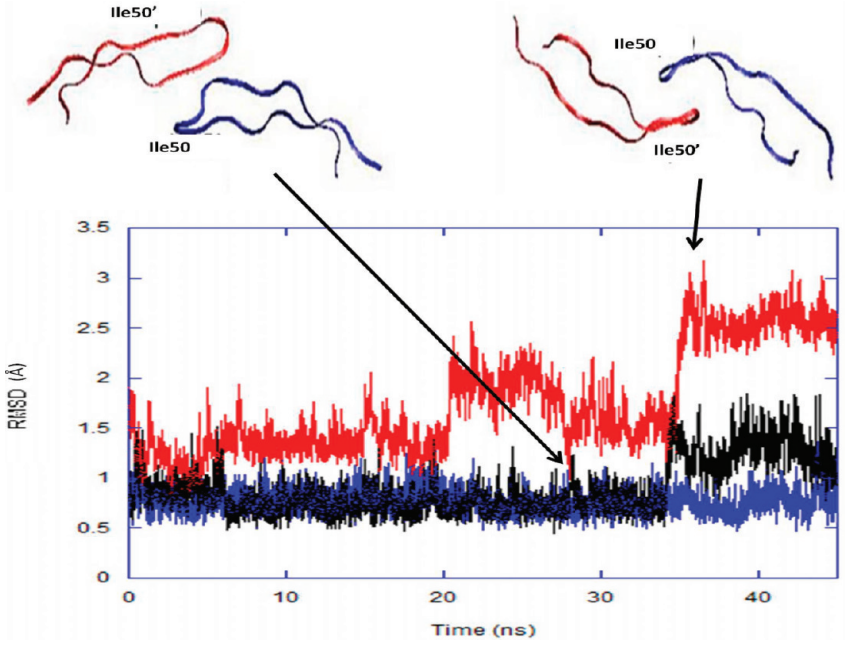

Figure 3. rmsd of flaps for bound (darunavir in blue, fullerene in red) and apo HIV-1 PR (in black), all structures starting from the closed state and overlapped on the crystal structure of closed HIV-1 PR (2IEN). The relative orientation of the flaps for the fullerene–HIV-1 PR complex is reversed between semiopen and closed states (top).

computations feasible. Darunavir was treated as one subsystem, and the surrounding environment was the other one. The interacting subsystems are presented schematically in Figure S2. The drug environment includes the following amino acids: Arg8, Leu23, Asp25-Trh26-Gly27-Ala28-Asp29-Asp30, Gly48-Gly49-Ile50, Pro81-Val82, Ile84, Leu23′, Asp25′-Thr26′-Gly27′-Ala28′-Asp29′-Asp30′, Gly48′-Gly49′-Ile50′, Pro81′-Val82′, Ile84′, and three water molecules. Computations were performed at the RHF/6-31G level of theory, and 2535 contracted Cartesian Gaussian basis functions were employed to describe the whole system. Due to the size of the system, we have not attempted to determine interaction energy components resulting from the partition of the correlation energy at the MP2 level of theory (i.e., uncoupled dispersion energy, correlation correction to electrostatic energy, and exchange–delocalization term).[95]

RESULTS AND DISCUSSION

Structural Stability in Darunavir–HIV-1 PR and Fullerene–HIV-1 PR Complexes. MD simulations for the two (darunavir and fullerene) bound forms and for the ligand-free HIV-1 PR were initiated with the same closed structure of the protease (2IEN). The use of the crystal structure as starting conformation for darunavir into HIV-1 PR was rationalized by clustering calculations for the drug in aqueous solution: dominant darunavir conformations in water resembled its crystal structure, with average root-mean-square deviation (rmsd) = 3.2 Å (Figure S3). The trajectory obtained for darunavir–HIV-1 PR showed a stable structure with the drug inside the cavity and the flaps being close to each other. The high degree of stability for the protease is indicated by the rmsd values for HIV-1 PR in bound and apo forms (Figure 2a): a Cα-based rmsd calculation with respect to the crystal structure of the protease yielded average values of 1.07 Å and 1.11 Å for

dx.doi.org/10.1021/ci300014z | J. Chem. Inf. Model. XXXX, XXX, XXX–XXX

darunavir−HIV-1 PR and unbound HIV-1 PR, respectively, suggesting that no important structural changes occurred during the simulation. During the last 15 ns however, rms deviations at the protease were greater in the case of the unbound system; such a behavior may arise from flap-opening events that occurred in the apo form of HIV-1 PR. In contrast, HIV-1 PR appeared less stable upon fullerene docking, with relatively pronounced conformational changes at ≈20 ns and ≈35 ns that yielded an average 1.49 Å rmsd (Figure 2a, red).

While the structure of the darunavir-protease complex remained overall stable, certain regions of the protease presented differences in flexibility. Cα atomic fluctuation calculations for each residue of HIV-1 PR revealed that residues such as the catalytic Asp25/25′ present a low degree of flexibility in the darunavir−HIV-1 PR complex (≈0.4 Å, Figure 2b), while they appear slightly more flexible in the free-protease system (≈0.6 Å), and along with Thr26/26′ and Gly27/27′ they belong to the most stable region of the protease. Fluctuations computed for the fullerene complex further supported the aforementioned statement (≈0.5 Å for Asp25/25′, very low values for Thr26/26′, Gly27/27′ as well, Figure 2b). This renders the catalytic triad as a candidate for substrate-protease interactions. HIV-1 PR residues appeared equally flexible in the apo and darunavir-bound forms, with the exception of the flap regions, which presented higher mobility in the unbound form, thus rationalizing the previously discussed increase in rmsd of the apo HIV-1 PR. Flap tip residues (Ile50/50′) of darunavir-bound HIV-1 PR showed a high stability (fluctuations <0.6 Å), suggesting that the flaps remain closed on top of the drug, whereas in the fullerene-bound form they are the most flexible parts (especially Ile50 with fluctuation of 2.8 Å).

An interesting behavior was observed regarding flap rms deviations for the darunavir/fullerene-bound and apo protease forms. Calculations have been carried out for the flaps [rmsd on Cα of residues 43−58 (chain A) and 43′-58′ (chain B)] of both forms starting from the closed state and overlapped on the same state. rms values for the darunavir-bound protease were very low—and for the first 35 ns were very similar to the values calculated on the apo HIV-1 PR (average deviation 0.8 Å)—meaning that HIV-1 PR is found in its closed state (Figure 3). In contrast, the fullerene-bound protease flaps that were initially closed, converted to semiopen within 20 ns, and they occasionally revisited the closed state (at ≈28 ns and ≈33 ns) as shown by the corresponding rms values (Figure 3, red). Each conversion of the unbound form from the closed to the semiopen state is followed by the reversion of the relative orientation of the flaps or "handedness" (Figure 3, top). Hornak et al. have also observed rmsd values ≈3 Å between closed and semiopen forms of HIV-1 PR.[3] Our previous analysis suggested that the reversion of handedness observed in fullerene−HIV-1 PR was the main cause of the increased flap flexibility and rms deviation in this complex. However, the flaps in fullerene−protease complex did not acquire an open conformation and similarly to the darunavir-bound HIV-1 PR they remained on top of the ligand, thus entrapping it permanently inside the cavity.

HIV-1 PR Flap Dynamics and Hydrogen Bonding Interactions: The Role of Water. The distance between the two Cα atoms of the isoleucine flap tips has been indicated as a reasonable way to describe the extent of flap opening.[3] The average flap distances for the darunavir-bound, the fullerene-bound, and the free HIV-1 PR complexes are 5.8 Å, 7.1 Å, and 6.2 Å, respectively (Figure S4a). In the case of fullerene-bound protease we observed that although for most of the time the distance between flaps remained stable (close to the average 6 Å), a spontaneous flap separation to 10 Å occurred after 35 ns; as observed above, this may have occurred due to the reversion of the handedness. Previous studies have shown that extensive flap opening (≈20 Å) is required for conformational changes that lead to ligand binding or release.[16] This further denoted the role of the flaps to restrain the fullerene inside the binding cavity throughout the simulation. Even though flaps in fullerene−HIV-1 PR are further apart toward the end of the simulation and appear flexible, they were close enough not to allow substrate escape. By contrast, a permanent, tight approach of the flaps was observed for the darunavir−HIV-1 PR system, indicating a compact and stable structure of the protease induced by the presence of the drug. Also, flaps in the free protease acquired the semiopen conformation after ≈37 ns.

Hydrogen bonding analysis on the flap region (residues 47-54 and 47′-54′) of the darunavir complex revealed the existence of a permanent HB interaction (91% occupation with respect to time) between backbone Ile50′ and Gly51, which stabilized the flaps above darunavir (Table 1 and Figure 4a). A similar interaction was observed for the fullerene-bound HIV-1 PR (Ile50−Ile50′), which lasted for the first 35 ns and was eventually replaced by a HB between Ile50 and Gly51′ for the last part of the simulation. This suggested that in both cases the flaps bind the ligand, despite the larger distance separating the flap tips of the fullerene-bound complex. On the other hand, an HB between the two flaps Ile50′ and Gly51 is present for 69% of the simulation in the case of the apo HIV-1 PR, well rationalizing the relatively unstable structure of the flaps at the end of the simulation. A striking observation was the role of a water molecule to mediate the flap tips in darunavir−HIV-1 PR: a very frequent, dual interaction between the water molecule and each of the flap tips (Ile50 and Ile50′) stabilized further the flap structure above darunavir in a closed conformation (Figure 4a). The absence of an analogous HB bridge in the free protease and in the fullerene-bound system suggested the influence of the flaps in effective binding and implicated the water as a crucial flap-stabilizing factor.

Table 1. Main Interactions Involving Hydrogen Bonds between the Flaps of HIV-1 PR

	occurrence[b]		
interaction[a]	darunavir−HIV-1 PR	fullerene−HIV-1 PR	apo HIV-1 PR
Ile50′ O-Ile50 N-H	6.4%	71.6%	9.5%
Ile50′ O-Gly51 N-H	91.4%		68.5%
Ile50′ O-Gly52 N-H	17.0%		12.2%
Gly51′ O-Ile50 N-H		16.0%	
H_2O-Gly51 N-H			14.8%
H_2O-Ile50 N-H	82.4%		
H_2O-Ile50′ N-H	97.7%	8.1%	

[a]N and O refer to backbone nitrogen atoms and carbonyl oxygen atoms, respectively. [b]Occurrence is defined as the percentage of simulation time that a specific interaction exists; interactions occurring less than 5% of the simulation are not shown.

Hydrogen Bonding Interactions between Darunavir and Binding Cavity Residues. Darunavir was stabilized inside the cavity of the protease by a strong HB network, which involves interactions among the hydroxyl group, 4-amino

dx.doi.org/10.1021/ci300014z | J. Chem. Inf. Model. XXXX, XXX, XXX−XXX

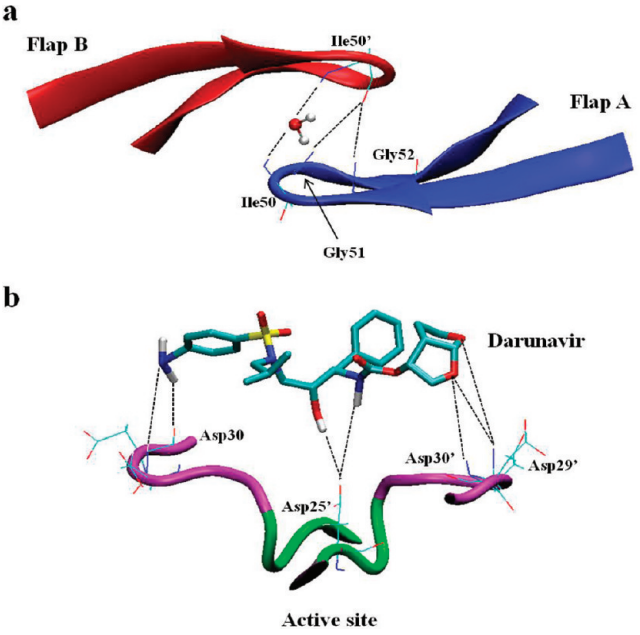

Figure 4. Hydrogen bonds between (a) the two protease flaps: a water molecule bridges backbone flap tips Ile50 and Ile50 in a closed conformation over darunavir and (b) darunavir and binding cavity residues of HIV-1 PR: seven principal interactions involving residues Asp29′, Asp30/30′, and Asp25′ stabilize darunavir inside the protein. For simplicity, only polar hydrogen atoms of darunavir are displayed.

phenyl moiety, *bis*-THF moiety in darunavir and active site (Asp25′) or near to active site (Asp29/29′, Asp30/30′) residues in HIV-1 PR (Table 2). A constant interaction between the hydroxyl group in darunavir and the side chain of catalytic Asp25′ is complemented with several interactions between the N−H group (of 4-amino phenyl moiety) and backbone atoms in residues Asp29/30 (chain A) as well as between oxygen atoms in the *bis*-THF moiety with backbone Asp29′/30′ (chain B) to induce a very stable structure for the darunavir−HIV-1 PR complex. A graphical representation of the HBs between darunavir and the protease is given in Figure 4b.

The design of first-generation clinical inhibitors[20] (Figure S5: saquinavir, indinavir, ritonavir, nelfinavir) was based on enhanced HIV-1 PR−ligand interactions (mainly HB and hydrophobic contacts) as evolved from the crystal structures of previous peptidic inhibitors.[32,96] All drugs combine peptide-like carbonyl groups and amides that form conserved HBs, with large hydrophobic groups to attain high affinity for HIV-1 PR; also similarly to darunavir, they involve a central hydroxyl group directly interacting with the active site aspartic acids of the protease. The first clinical inhibitor, saquinavir, has three peptide-like HBs with the backbone of the protease (Asp29′/30′, Gly48′) as well as water-mediated interactions with the amides of flap tips (Ile50/50′). Enhanced hydrophobic interactions between saquinavir and HIV-1 PR are also present due to the large side groups of the drug. Todd et al. have also shown that HIV-1 PR inhibition by saquinavir is mainly driven by the entropic contribution.[97] Efforts to reduce the molecular weight and peptidic character of saquinavir led to the discovery of nelfinavir. Nelfinavir possesses a phenolic OH group that directly interacts with Asp30 of the protease. A hydrogen bond between an NH and the backbone of Gly27 also stabilizes nelfinavir inside the binding cavity. The other NH group of nelfinavir is associated with a water molecule that interacts with the amide group of Asp29′. The problem of drug resistance however has emerged the development of new antiviral drugs, since drug-resistant mutations alter the shape and size of HIV-1 PR subsites, thus dramatically reducing the affinity. In addition, the peptide-like character of the "first-generation" inhibitors caused several shortcomings such as poor bioavailability, low metabolic stability, side effects, and heavy pill burden.[98] The new inhibitors (lopinavir, atazanavir, amprenavir, fosamprenavir, tipranavir, darunavir)[20] present fewer peptidic characteristics: in tipranavir, amprenavir, and darunavir, the carbonyl group was replaced by a sulfonamide group and tetrahydrofuran (THF) and *bis*-tetrahydrofuran (*bis*-THF) groups were added to amprenavir and darunavir, respectively, to introduce nonpeptidic HB candidates.[99] Lopinavir was developed to overcome resistance problems associated with ritonavir, in particular with ritonavir-resistant proteases due to mutations at residue V82.[100] Lopinavir's interactions in HIV-1 PR active site involve residues Asp25/25′ (side chain, carboxyl oxygen atoms), Gly27/27′ (backbone carbonyl oxygen atoms), and Asp29 (backbone amide and carboxyl oxygen). Despite the enhanced binding features of lopinavir that lead to its good antiviral activity, it was apparent that it suffers from poor

Table 2. Principal Hydrogen Bonding Interactions between Darunavir and HIV-1 PR[a]

Interaction[a]	
Darunavir–HIV-1 PR	Occurrence[b]
O3-H33–Asp25' OD2	100.0%
N1–Asp30 N-H	90.8%
N1-H37–Asp30 O	90.5%
O7–Asp29' N-H	86.5%
O6–Asp30' N-H	81.0%
N3-H31–Asp25' OD2	79.6%
O6–Asp29' N-H	51.4%
N1–Asp29 N-H	19.7%

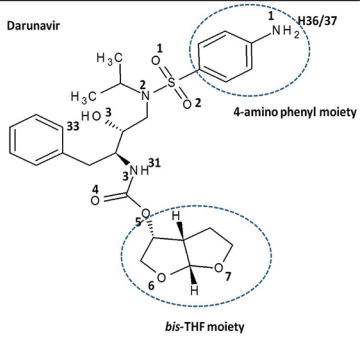

[a]Notes: [a]N and O refer to HIV-1 PR backbone nitrogen atoms and carbonyl oxygen atoms, respectively; OD2 is a carboxyl oxygen atom. [b]Occurrence is defined as the percentage of simulation time that a specific interaction exists; interactions occurring less than 10% of the simulation time are not shown.

dx.doi.org/10.1021/ci300014z | J. Chem. Inf. Model. XXXX, XXX, XXX−XXX

bioavailability, similarly to the first-generation PIs. To improve on this, atazanavir was developed in the late 1990s. In addition to the aforementioned HBs in the lopinavir−HIV-1 PR complex, atazanavir is involved in interactions with the backbones of Gly48/48′ and Asp25′. Amprenavir bears a tetrahydrofuranyl oxygen atom that interacts with the backbone amides of Asp29 and Asp30. It has also interactions with Asp25/25′ and with a water molecule between the flaps. Tipranavir participates in an HB network, which involves the highly conserved backbone atoms of Asp29/30, Gly48, and Ile50/50′. In contrast with other PIs, tipranavir's interaction with the flap tips Ile50 and Ile50′ is not bridged via a water molecule. This direct interaction may account for the gain in binding entropy observed in the tipranavir−HIV-1 PR complex (ΔS = −14.6 kcal mol^{-1}). A small, yet favorable enthalpy change also contributes to tipranavir binding (ΔH = −0.7 kcal mol^{-1}).[101] Furthermore, the OH group of tipranavir participates in HB with the side chains of Asp25/25′, and several hydrophobic interactions contribute to the drug's exceptional antiviral activity and resistance profile.

Similarly to darunavir, in all PIs it is apparent that strong inhibitor−active site HB interactions are necessary. The presence of a water molecule to stabilize the flaps of the protease is also important; however, strong inhibitors such as tipranavir appear to induce a closed conformation of the flaps via direct interactions.

One of the most serious problems in AIDS treatment is the development of resistance due to the high mutation rate in HIV replication that ultimately renders the HIV-1 PR inhibitor drugs ineffective.[20] Despite the superiority of darunavir to other clinical PIs,[102] the appearance of mutations that confer resistance to all available PIs is still a great challenge in treating HIV.[24] It is encouraging, however, that the backbone conformation of the active site undergoes very little change upon viral mutations. Based on this feature, the introduction of conserved HBs between darunavir and backbone atoms of the protease has been very successful against resistant HIV.[9] Thermodynamic, kinetic, and crystallographic studies have verified the great effectiveness of darunavir on drug-resistant mutants of the protease.[20] Despite that major darunavir resistance-associated mutations (RAM) have been identified to include V32I, I50V, I54M/L, L76V, and I84V,[103,104] previous findings have demonstrated that darunavir efficacy remains excellent. This is mainly due to the low occurrence of RAM in darunavir as well as its high genetic barrier (a large number of mutations is required to significantly reduce darunavir's affinity for HIV-1 PR). Tie et al. have studied darunavir complexes with HIV-1 PR mutants V82A and I84V.[8] Crystal structures showed minor structural changes, with K_i values of the mutant complexes being similar to the WT ones. Additionally, darunavir has been also implicated in the inhibition of HIV-1 PR dimerization.[105]

However, specific drug resistance mutations of residues in the binding cavity may alter the interactions with darunavir. Thus, darunavir−HIV-1 PR complexes with mutations D30N, V32I, I50V, and I84V displayed reduced interactions compared to the WT complex.[8,22] Particularly in the I50V variant, HIV-1 PR has reduced van der Waals interactions with darunavir relative to the WT. The I50V mutation also destabilizes significantly the interactions at the interface between the two subunits, resulting in a lower stability of the PR dimer.[106] A similar loss of intersubunit interactions has been observed in different studies referring to mutations L24I and F53L.[106,107] Additionally, it was observed that mutation I54V causes the loss of the water bridge between flap tips.[108]

The Fullerene-Bound Complex Resembled the Darunavir-Induced Compact Structure of HIV-1 PR. Darunavir−HIV-1 PR presented a stable flap−active site distance with average 14.7 Å (Figure S4b), very similar to the free protease (average = 13.8 Å). This distance for fullerene−HIV-1 PR showed a random distribution, as a result of the increased Ile50 flap flexibility. During the first 35 ns, the fullerene-bound protease was found in a relatively tight conformation with the Ile50−Asp25 distance slightly fluctuating around 16.5 Å, while later the distance gradually increased to reach values up to 22 Å. Importantly, for the most part of the simulation the flap−active site distance was very stable and similar for the apo and darunavir-bound HIV-1 PR; however, a shift of the flaps toward the active site of the protease was not observed in darunavir−HIV-1 PR. This may suggest that such a shift of the flaps may not be required for effective binding as it has been suggested by previous studies.[11,12] Instead, a tight and stable flap conformation is rather necessary for a strong binding effect.

To organize our findings in a more condensed scheme we investigated the correlation between flap distance and flap−active site distance that defines the probability of finding the protease cavity in different conformations. The optimal combination corresponds to a representative protease structure for the binding state. Thus, in Figure 5 we observed the

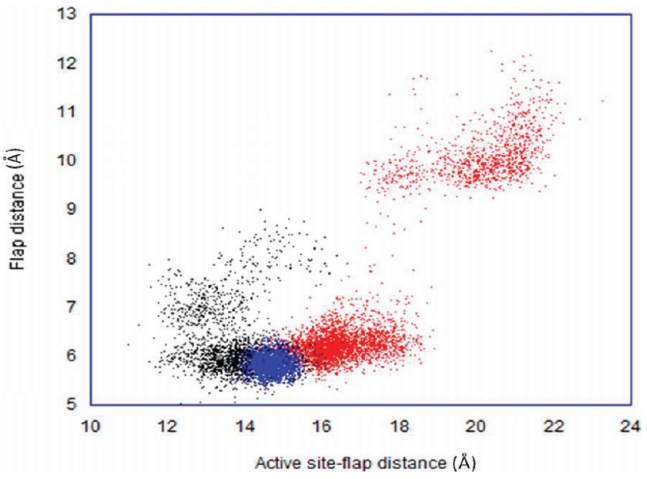

Figure 5. The size of the HIV-1 PR cavity in darunavir−HIV-1 PR (blue), fullerene−HIV-1 PR (red), and apo HIV-1 PR (black), as defined by the combination of the flap (Ile50−Ile50′) distance with the flap−active site (Ile50−Asp25) distance.

corresponding areas for all systems. The values for the darunavir complex indicated a closed (short flap distances and active site-flap distances) and stable (all points concentrated in a small area) structure, with the corresponding region for the free protease showing a less tight structure for the cavity, as expected by the greater flexibility of the unbound system. The fullerene-bound complex displayed two main conformations for the binding cavity, with the most populated one resembling the size of the cavity upon darunavir entrapment. From these plots the role of the highly potent darunavir to induce a compact structure of the protease becomes apparent: strong interactions between the drug and residues of the protease stabilized HIV-1 PR, thus resulting in an efficient inhibitory effect. However, the fullerene also

dx.doi.org/10.1021/ci300014z | J. Chem. Inf. Model. XXXX, XXX, XXX−XXX

resulted in similar structural rearrangements, as expressed by protease's conformational changes. It could be then suggested that tight-cavity structures do not necessarily indicate effective binding, since such conformations may be induced by inert ligands or even in the absence of a ligand. Flap stabilization over the substrate (even if it results in a more "expanded" structure of the cavity) is a more crucial factor regarding effective binding.

Protease Structural Changes Anticipated in Effective Binding May Also Arise by the Presence of an "Inert" Ligand. Upon fullerene docking into HIV-1 PR, the former remained roughly in the center of the cavity during the whole simulation with average distances between each fullerene atom and the Asp25 catalytic site ranging from 8.4 Å to 13.3 Å (fullerene atoms−Asp25 Cα). Even though the fullerene was entrapped into the cavity during the simulation, the fullerene−active site distance was rarely less than 6.5 Å, thus excluding the possibility of HB formation between the substrate and the active site. This was expected since the fullerene is lacking any regions with significant differences in electronegativity that might be potential candidates for HBs with neighboring protease residues. MM−PBSA analysis for the fullerene−HIV-1 PR complex revealed that the selected compound is indeed an ineffective HIV-1 PR inhibitor with large binding energy, ΔG_{bind} = −3.5 kcal mol^{-1} (Table 3). Binding energy

Table 3. MM−PBSA Energies for the Fullerene−HIV-1 PR Complex (kcal mol^{-1})

	energy	±SEM[a]
ΔE_{elec}	0.42	0.03
ΔE_{vdW}	−69.45	0.06
ΔE_{MM}	−69.03	0.08
ΔG_{NP}	−6.72	0.00
ΔG_{PB}	19.75	0.04
ΔG_{solv}	13.03	0.04
$\Delta G_{elec(TOT)}$ $=\Delta E_{elec}+\Delta G_{PB}$	20.17	0.04
$\boldsymbol{\Delta H_{(MM+solv)}}$	−56.00	0.07
$-T\Delta S_{TOT}$	52.48	0.17
$\boldsymbol{\Delta G_{bind}}$	−3.52	0.18

[a]Standard error of the mean (SEM) values: SEM = standard deviation/$\sqrt{N}$, with N being the number of trajectory frames used in MM−PBSA calculations (450 for entropy and ΔG_{bind}, 4500 for everything else).

decomposition implicated the electrostatics and the entropic contribution as the main reasons for unfavorable binding. However, strong van der Waals interactions (ΔE_{vdW} = −69.5 kcal mol^{-1}) and the nonpolar contribution to solvation (ΔG_{NP} = −6.72 kcal mol^{-1}) contributed favorably toward permanent enclosing of the fullerene into the binding cavity. Interestingly, ΔE_{vdW} and ΔG_{NP} for fullerene−HIV-1 PR are comparable to darunavir−HIV-1 PR, according to Hou et al. ($\Delta E_{vdW,darunavir}$ = −66.8 kcal/mol and $\Delta G_{NP,darunavir}$ = −9.4 kcal/mol).[44] The significantly enhanced electrostatic interactions and less unfavorable entropy change in the darunavir complex ($\Delta E_{ele,darunavir}$ = −41.7 kcal/mol and $-T\Delta S_{darunavir}$ = 26.0 kcal/mol, compare with Table 3) than in the fullerene complex are the main reasons for the minor efficacy of the fullerene against HIV-1 PR. This is not surprising, as in most PIs the binding energy of darunavir also comes primarily from the entropy change due to water depletion from the binding cavity.[24]

rmsd values for the fullerene supported its low flexibility into HIV-1 PR, with negligible fluctuations around the average of 0.2 Å, thus picturing the fullerene as practically static inside the cavity (Figure S6). Similarly, darunavir appeared very stable, primarily due to the HBs with cavity residues. Thus, it was suggested that a strongly hydrophobic substrate with favorable van der Waals interactions and nonpolar contribution to solvation may induce conformational changes to the protease that accompany effective binding even if it is a very poor inhibitor.

To further investigate the role of the two ligands in binding, we have calculated their SASA values inside the cavity. Previous experimental and theoretical studies have identified the surface, which becomes desolvated upon binding, as being mainly hydrophobic.[32] The active site of HIV-1 PR is almost cylindrical, consisting primarily of hydrophobic amino acids. Friedman et al. developed computational approaches to increase the hydrophobic desolvation of fullerene-based inhibitors relative to previously tested compounds.[109] This resulted in significantly higher binding affinity (≈50-fold increase) of the designed fullerenes for HIV-1 PR. We have constructed the histogram of SASA values for darunavir and for the fullerene (Figure S7) to observe that the two distributions differ in their range, with average SASA for the drug and for the fullerene being 77.49 Å^2 (narrower distribution) and 107.93 Å^2 (broader distribution), respectively. The broader distribution of SASA values for the fullerene implies that the aqueous environment around the fullerene changes more frequently than the solvent environment around darunavir. As we observed above, the greater flexibility of Ile50 flap may control fullerene exposure to solvent by inducing multiple flap transitions between closed and semiclosed states. To obtain a direct comparison of the SASAs around the fullerene and darunavir, we have also calculated the values for each ligand in the absence of the protease. Total surface areas for the solvated fullerene and darunavir have been computed to be 606.93 Å^2 and 749.76 Å^2, respectively, rendering the fullerene more solvent-accessible inside the cavity than darunavir: indeed, the relative SASA [(SASA for compound inside the cavity)/(total surface area of compound)] values for the two systems are 17.8% for the fullerene and 10.3% for darunavir. This finding denotes the ability of darunavir to exclude water molecules from the binding cavity, and it may be of additional support regarding the stability of the darunavir−HIV-1 PR system. Fullerenes are strongly hydrophobic compounds and are anticipated to increase hydrophobic desolvation in HIV-1. The significant water depletion, however, is probably compensated by the lack of electrostatic interactions inside the cavity and by the aforementioned structural rearrangements of the flaps that induce significant solvent exposure to the fullerene.

Ligands Followed an Alternative Pathway To Enter the HIV-1 PR Cavity. We next considered the entering pattern of each ligand by choosing several different poses as initial conformations, with respect to the flap tips. In particular, we have selected the open crystal structure 1TW7 to manually place the compounds in 15 random positions near the open region. We monitored the main patterns that govern the entering process, namely the interactions between the ligand and the flaps during that time. Conformations initiated between the flaps rapidly entered the cavity followed by flap closing, whereas poses being outside of the flaps presented various outcomes: they were either excluded from the binding cavity

dx.doi.org/10.1021/ci300014z | J. Chem. Inf. Model. XXXX, XXX, XXX−XXX

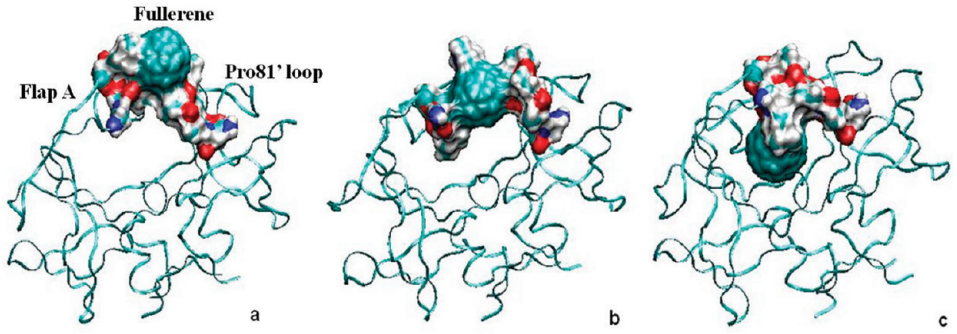

Figure 6. Alternative entering process for the fullerene into the binding cavity of HIV-1 PR: (a) The fullerene approaches the flap-loop channel, (b) access to the binding pocket is obtained via channel opening, and (c) the fullerene settled into the cavity with subsequent channel closing. Residues 48−52 (flap A), 79′-83′ (Pro 81′ loop), and the fullerene are represented as surfaces.

after the closing of the flaps or they eventually entered the interior of the protease before flap approach. An interesting entering pattern was observed, however, for one pose that followed a different course to approach the cavity, while flaps had been already closed. Among all entering modes, only the latter has been included in our analysis. Initial structures for the fullerene and darunavir systems are given in Figure S1, with the fullerene being outside the protease cavity, at a distance 10.7 Å from the chain A flap tip (defined as the distance between the nitrogen atom on fullerene and the Cα on Ile50). In that particular case, upon beginning of the simulation the fullerene rapidly reorients (within 30 ps) to facilitate its entrance to the cavity and attacks the open site of the protease. By that time, the flap tips have been already closed and remained in this state for ≈0.5 ns with an average distance between them 6.5 Å. It is worth noting that we have monitored the rate of flap closing for the open HIV-1 PR to be a very fast procedure that is realized within 50 ps. Thus, it was not expected for the fullerene to enter the cavity unless the flaps eventually open. Indeed, the flaps fluctuated toward the open state for the next 0.5 ns. Nevertheless, the flap opening was not sufficient for the fullerene to enter. Unexpectedly, at ≈1 ns the fullerene began to approach the binding cavity with the flaps being practically closed; it attacked HIV-1 PR from a region formed between the one flap (Ile50, chain A) and the (Pro79′/Thr80′/Pro81′/Ala82′/Asn83′, chain B) loop (Figure S8). Eventually, the compound entered the binding cavity and remained inside the protease for the remaining of the simulation. The interaction between HIV-1 PR and the fullerene during the entering process is depicted in Figure 6, where protease residues 48-52 and 79′-83′ and the fullerene are represented as surfaces. The fullerene was initially positioned in a groove formed between the flap and loop areas (Figure 6a). The channel eventually opened to accommodate the ligand (Figure 6b), before it reshaped to a closed structure (Figure 6c). We have also observed that darunavir followed the same procedure to approach the cavity. These findings illustrate the possibility of alternative (substrate-unrelated) entering pathways into the binding cavity of HIV-1 PR. This suggested that flap opening might not be necessary for ligand access to the cavity.

Intermolecular Interaction Energy Partitioning. The total intermolecular interaction energy for darunavir−HIV-1 PR obtained at the RHF level of theory was −20.19 kcal mol^{-1} (Table 4). As noted above, the existence of multiple HBs between darunavir and the surrounding environment suggested that electrostatics should be important. Indeed, this value was quite large (−95.38 kcal mol^{-1}). However, as it has been

Table 4. Energy Components (kcal mol^{-1}) Determined at the RHF/6-31G Level of Theory

interaction	$\varepsilon^{(10)}_{el}$	ε^{HL}_{ex}	ΔE^{HL}[a]	ΔE^{HF}_{del}	ΔE^{HF}
HIV-1 PR−darunavir complex	−95.38	111.35	15.97	−36.16	−20.19

[a] $\varepsilon^{HL}_{ex} + \varepsilon^{(10)}_{el} = \Delta E^{HL}$.

recently shown by some of us[92,93] as well as by others,[110] in the case of hydrogen-bonded complexes the stabilization due to the mutual polarization of interacting subsystems reflected on the large value of delocalization component (ΔE^{HF}_{del}; encompassing induction terms) is also important. Moreover, the intermolecular interaction partitioning indicated that although first-order electrostatics is substantial, it is completely quenched by the associated Pauli repulsion (111.35 kcal mol^{-1}). The latter contribution cancels out partially the delocalization term. Therefore, even at the uncorrelated level of theory the picture is quite complicated.

Although in the case of the darunavir complex typical stacking motifs were not present between darunavir and neighboring amino acids, it follows from previous studies that one might expect non-negligible additional stabilization resulting from the dispersion component of the interaction energy.[92,110]

Molecular Dynamics of Darunavir in DMPC. To simulate the structural behavior of darunavir into a lipid membrane we have performed an MD study of the drug, initially placed outside the DMPC bilayer. It was observed that darunavir entered the bilayer within 80 ns and remained inside for the remaining 160 ns of the simulation. An important structural property of a lipid bilayer system is the area per lipid, which is defined by the product of X and Y dimensions of the simulation box divided by the number of lipids present in each monolayer (64 lipids in our case). Experimental and simulation results vary between 0.60 nm^2 and 0.67 nm^2.[111−115] In this case, the values for the area per lipid A are presented in Table 5, and they did not change with the concentration of darunavir.

The distribution of components along the normal to the bilayer (Z-axis) is presented in Figure 7a, in which all density profiles are depicted. Obviously, darunavir prefers being in the interior of the bilayer although it was initiated outside. Focusing on the headgroup of lipids, the angle between the vector connecting P and N atoms (Figure S9a) and the Z-axis is of great importance. The presence of darunavir (either one or five molecules) did not affect significantly the values of the aforementioned angle as seen in Table 5. In Figure S9b, a

dx.doi.org/10.1021/ci300014z | J. Chem. Inf. Model. XXXX, XXX, XXX−XXX

Table 5. Properties of the Water−DMPC−Darunavir System: Area per Lipid (A), Lateral Diffusion Constant (D_L), and Angle between the PN Vector and the Z-axis (θ_{P-N})

	number of molecules	
property	1	5
A [nm^2]	0.632 ± 0.003	0.633 ± 0.005
D_L [10^{-7} cm^2/s]	0.54 ± 0.15	2.38 ± 0.7
θ_{P-N} [degrees]	79.6 ± 0.2	78.3 ± 0.3

configuration of five darunavir molecules into DMPC is presented.

It was also shown that darunavir was involved in HBs with lipid and water molecules. A quantitative estimation of the HBs between darunavir and the other components of the system is given in Table S2. Darunavir forms on average four HBs with DMPC and one with a water molecule, thus acquiring a stable conformation inside the bilayer.

Concerning the hydrophobic part of the lipids, the deuterium order parameter ($-S_{CD}$) of the alkyl tails, which is a measure of ordering, is given by the following equation

$$-S_{CD} = \frac{2}{3}S_{xx} + \frac{1}{3}S_{yy} \tag{8}$$

The components on the rhs of the above equation are computed by the tensorial formula

$$S_{ij} = \frac{1}{2}\langle 3\cos\theta_i\cos\theta_j - \delta_{ij}\rangle \tag{9}$$

where θ_i is the angle between the i^{th} molecular axis and the bilayer normal. The molecular axes for the n^{th} methylene group are defined as follows. z: vector from c_{n-1} to c_{n+1}, y: vector normal to z and in the plane through c_{n-1}, c_n, and c_{n+1}, x: vector normal to z and y.[50,55] The order parameters presented in Figure 7b were averaged over the two alkyl tails of DMPC, and they are slightly shifted upward as the number of drug molecules increases.

The lateral diffusion of darunavir molecules is extracted from the mean square displacement (MSD) plots. In particular, the lateral diffusion constant is estimated as

$$D_L = \frac{D_{xx} + D_{yy}}{2} \tag{10}$$

The components in the rhs of eq 10 are the self-diffusion constants along the X and Y axes, and they are described by Einstein relations such as the next one

$$D_{xx} = \lim_{t\to\infty} \frac{\langle (x_i(t) - x_i(0))^2\rangle}{2t} \tag{11}$$

where x_i is the x coordinate of the darunavir center of mass. A similar equation holds for the self-diffusion constant along the Y-axis substituting the x positions with the y ones. The values of the lateral diffusion constant of the drug are given in Table 5 for all systems.

The rmsd of darunavir, compared with its crystal structure has been also monitored. Figure 7c shows the rmsd over the last 100 ns of the simulation denoting the structural stability of darunavir. Regarding the higher concentration of the drug (five molecules), no crossing events (to reach the opposite leaflet) were observed up to 240 ns. This is shown in Figure 7d, where the Z-distance between the darunavir and the bilayer centers of mass is depicted. The zero in Z-axis corresponds to the center of mass of the bilayer.

As mentioned above, darunavir adopted a stable structure into DMPC via HB interactions with the bilayer and water molecules. Thus, clustering calculations yielded a representative

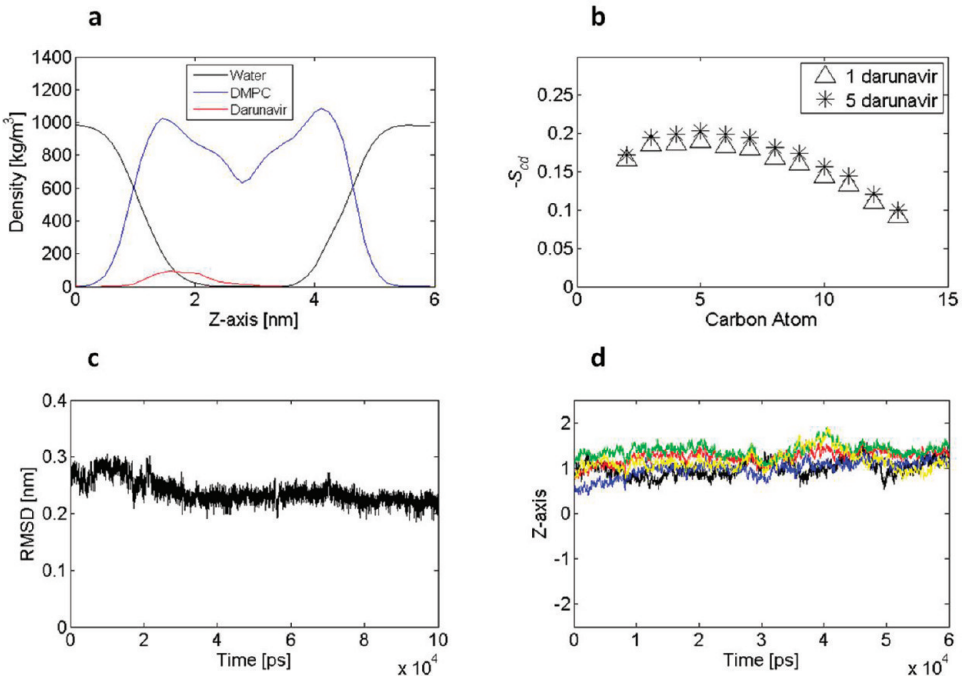

Figure 7. (a) Density profiles along the Z-axis for the bilayer, water, and five darunavir molecules; (b) deuterated order parameters for the alkyl tails of DMPC in the presence of darunavir; (c) rmsd of one darunavir molecule with respect to the crystal structure, over the last 100 ns of the simulation; (d) distance between the darunavir and bilayer centers of mass. Each darunavir molecule is in a different color. No crossing events were observed.

dx.doi.org/10.1021/ci300014z | J. Chem. Inf. Model. XXXX, XXX, XXX−XXX

structure for the drug into DMPC, which resembled its crystal structure with a difference on the orientation of the 4-amino phenyl moiety that resulted in a less extended conformation (Figure 8). Interestingly, the structure of darunavir into the bilayer also resembled its dominant conformation when bound to HIV-1 PR.

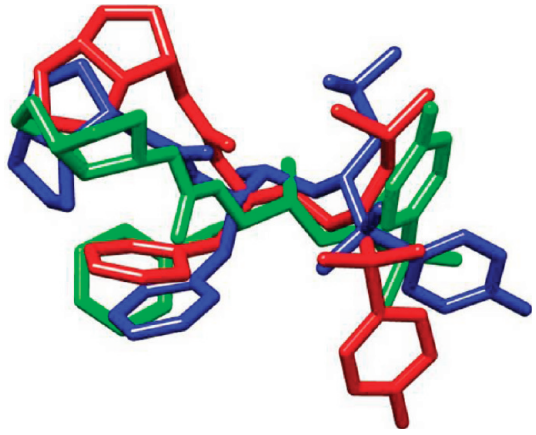

Figure 8. Representative structures of darunavir into HIV-1 PR (crystal structure, blue), HIV-1 PR (after 45 ns MD simulation, red), and DMPC (green).

CONCLUSIONS

We have compared the conformational properties and binding behavior of HIV-1 PR upon entrapping into the catalytic cavity either a potent drug (darunavir) or an "inert" fullerene derivative. We additionally initiated several poses for both compounds being outside the flap region of the protease to account for the role of the flaps as modulating factor of ligand-access to the cavity. 45 ns MD simulations in explicit solvent have been performed for the darunavir–HIV-1 PR crystal structure, for the fullerene–HIV-1 PR complex, and for the apo form of HIV-1 PR. Additionally, two 45 ns MD simulations in implicit solvent have been carried out for particular configurations of the fullerene and of darunavir being outside the flap tips of the "open" protease.

The darunavir-bound HIV-1 PR structure appeared very stable throughout the simulation with low rms deviations from the crystal structure. The most stable regions of HIV-1 PR were the two catalytic triads (Asp25/25′, Thr26/26′, Gly27/27′). In contrast, the protease appeared significantly flexible upon fullerene binding, mainly due to an increase in mobility of the flap in chain A (Ile50). The flaps in darunavir–HIV-1 PR were stabilized by HBs between Ile50′ and Gly51 as well as between Ile50 and Ile50′, which were mediated via a water molecule. The latter interaction was not observed in the fullerene-bound complex or in the free protease, thus denoting the importance of a H_2O-bridge in effective ligand-binding. Darunavir was also stabilized into HIV-1 PR via a strong HB network, which involved interactions among the hydroxyl group, the 4-amino phenyl moiety, the *bis*-THF moiety in darunavir, and active site (Asp25′) or near to active site (backbone Asp29/29′, Asp30/30′) residues in HIV-1 PR. Even though the flaps in fullerene–HIV-1 PR occasionally visited semiopen states due to their flexibility, they frequently resembled the "closed" conformation observed in the darunavir-bound protease mainly because of HB interactions between Ile50 and Ile50′. Despite the high mobility of Ile50, the flap tips remained primarily close to each other to keep the fullerene practically static inside the cavity for the entire simulation. Although significant van der Waals interactions and nonpolar contribution to solvation acted favorably toward fullerene–HIV-1 PR complex formation, MM–PBSA calculations showed that the fullerene is a poor protease inhibitor mainly due to its destabilizing electrostatic contribution. In contrast, QM calculations for a simplified darunavir–HIV-1 PR system implicated electrostatics as the most important factor of the intermolecular interaction energy. However, the size of the binding cavity upon fullerene entrapment was found comparable to the size of the cavity the most potent darunavir was accommodated into. This suggested that strong ligand-active site interactions may not be necessary for specific structural rearrangements that usually accompany binding (e.g., flap closing).

Also, the interaction between darunavir in different concentrations and a DMPC lipid bilayer was explored through large-scale MD simulations. Since darunavir acts inside the cell, it was of major importance to observe that the drug penetrated into the lipid phase and interacted with DMPC and water molecules via HBs. The preferred position of the drug was close to the headgroup region of the bilayer. Interestingly, darunavir into DMPC acquired similar conformations when bound to HIV-1 PR.

Finally, a remarkable feature was observed when MD simulations were initiated with the ligands outside the flap region. After the fullerene and darunavir were excluded from entering the cavity due to the rapid closing (within 50 ps) of the flaps, the flap tips remained permanently closed for several ns, not allowing access to protease's interior. The ligands used an (substrate-unrelated) alternative pathway (via an opening between Ile50 flap and Pro81' loop) to enter, making it questionable as to whether an Ile50–Ile50′ flap opening is necessary for a substrate to access the cavity.

From the above we arrived at the following conclusions on effective HIV-1 PR binding:

1) Structural stability of the protease flaps is more important than other conformational features (e.g., a tight cavity structure). Flexible flaps could present multiple conversions between closed and semiopen forms, thus permanently entrapping a *weak* inhibitor into HIV-1 PR cavity.
2) A water molecule, which serves as a HB bridge between flap tip residues Ile50 and Ile50′, is very important for inducing a "closed" and stable flap structure.
3) Enhanced inhibitor–backbone catalytic site HB interactions are important. It was observed that strong van der Waals interactions and the nonpolar contribution to solvation alone are not sufficient for effective binding. Electrostatics is the crucial component toward binding.
4) Ligand-access to the cavity is not necessarily controlled by flap opening. An alternative entering pathway may be realized through the region between the one flap of the protease and the Pro81′ loop.
5) Darunavir's conformation into DMPC resembles its structure into HIV-1 PR and is also involved in HB interactions with the bilayer and water molecules.

Significantly, conclusions 1–3 were also supported by observations on other PIs.

dx.doi.org/10.1021/ci300014z | *J. Chem. Inf. Model.* XXXX, XXX, XXX–XXX

■ ASSOCIATED CONTENT

Supporting Information

Nine additional figures showing 1) darunavir and fullerene initially placed outside the cavity of HIV-1 PR, 2) a representation of the two subsystems used in interaction energy decomposition, 3) the four clusters of darunavir in water, 4) flap distance and active site−flap distance for all systems, 5) FDA-approved protease inhibitors, 6) rmsd of darunavir and of fullerene inside HIV-1 PR, 7) SASA histograms, 8) the alternative entering pathway for the fullerene to HIV-1 PR, 9) darunavir into DMPC. Two additional tables showing 1) the partial charges for darunavir and fullerene atoms and 2) hydrogen bonds of darunavir into DMPC. This material is available free of charge via the Internet at http://pubs.acs.org.

■ AUTHOR INFORMATION

Corresponding Author

*E-mail: gleonis@eie.gr.

Notes

The authors declare no competing financial interest.

■ ACKNOWLEDGMENTS

This work was supported by funding provided by the European Commission for the FP7-REGPOT-2009-1 Project 'ARCADE' (Grant Agreement No. 245866). We also acknowledge the CINECA award under the ISCRA initiative, for the availability of high performance computing resources and support. Z.C. gratefully acknowledges the allotment of the CPU time granted by the Wroclaw Center of Networking and Supercomputing (WCSS). The study was supported by research fellowship within the "Development program of Wroclaw Medical University" funded from the European Social Fund, Human Capital, National Cohesion Strategy (contract no. UDA-POKL.04.01.01-00-010/08-00).

■ REFERENCES

(1) Brik, A.; Wong, C. H. HIV-1 protease: mechanism and drug discovery. *Org. Biomol. Chem.* **2003**, *1* (1), 5−14.

(2) Freedberg, D. I.; Ishima, R.; Jacob, J.; Wang, Y. X.; Kustanovich, I.; Louis, J. M.; Torchia, D. A. Rapid structural fluctuations of the free HIV protease flaps in solution: relationship to crystal structures and comparison with predictions of dynamics calculations. *Protein Sci.* **2002**, *11* (2), 221−232.

(3) Hornak, V.; Okur, A.; Rizzo, R. C.; Simmerling, C. HIV-1 protease flaps spontaneously open and reclose in molecular dynamics simulations. *Proc. Natl. Acad. Sci. U. S. A.* **2006**, *103* (4), 915−920.

(4) Nicholson, L. K.; Yamazaki, T.; Torchia, D. A.; Grzesiek, S.; Bax, A.; Stahl, S. J.; Kaufman, J. D.; Wingfield, P. T.; Lam, P. Y.; Jadhav, P. K.; Hodge, C. N.; Domaille, P. J.; Chang, C.-H. Flexibility and function in HIV-1 protease. *Nat. Struct. Biol.* **1995**, *2* (4), 274−280.

(5) King, N. M.; Prabu-Jeyabalan, M.; Nalivaika, E. A.; Wigerinck, P.; de Bethune, M. P.; Schiffer, C. A. Structural and thermodynamic basis for the binding of TMC114, a next-generation human immunodeficiency virus type 1 protease inhibitor. *J. Virol.* **2004**, *78* (21), 12012−12021.

(6) Koh, Y.; Nakata, H.; Maeda, K.; Ogata, H.; Bilcer, G.; Devasamudram, T.; Kincaid, J. F.; Boross, P.; Wang, Y. F.; Tie, Y.; Volarath, P.; Gaddis, L.; Harrison, R. W.; Weber, I. T.; Ghosh, A. K.; Mitsuya, H. Novel bis-tetrahydrofuranylurethane-containing nonpeptidic protease inhibitor (PI) UIC-94017 (TMC114) with potent activity against multi-PI-resistant human immunodeficiency virus in vitro. *Antimicrob. Agents Chemother.* **2003**, *47* (10), 3123−3129.

(7) Lefebvre, E.; Schiffer, C. A. Resilience to resistance of HIV-1 protease inhibitors: profile of darunavir. *AIDS Rev.* **2008**, *10* (3), 131−142.

(8) Tie, Y.; Boross, P. I.; Wang, Y. F.; Gaddis, L.; Hussain, A. K.; Leshchenko, S.; Ghosh, A. K.; Louis, J. M.; Harrison, R. W.; Weber, I. T. High resolution crystal structures of HIV-1 protease with a potent non-peptide inhibitor (UIC-94017) active against multi-drug-resistant clinical strains. *J. Mol. Biol.* **2004**, *338* (2), 341−352.

(9) Ghosh, A. K.; Chapsal, B. D.; Weber, I. T.; Mitsuya, H. Design of HIV protease inhibitors targeting protein backbone: an effective strategy for combating drug resistance. *Acc. Chem. Res.* **2008**, *41* (1), 78−86.

(10) Okimoto, N.; Tsukui, T.; Kitayama, K.; Hata, M.; Hoshino, T.; Tsuda, M. Molecular Dynamics Study of HIV-1 Protease-Substrate Complex: Roles of the Water Molecules at the Loop Structures of the Active Site. *J. Am. Chem. Soc.* **2000**, *122*, 5613−5622.

(11) Vondrasek, J.; Wlodawer, A. HIVdb: a database of the structures of human immunodeficiency virus protease. *Proteins* **2002**, *49* (4), 429−431.

(12) Lapatto, R.; Blundell, T.; Hemmings, A.; Overington, J.; Wilderspin, A.; Wood, S.; Merson, J. R.; Whittle, P. J.; Danley, D. E.; Geoghegan, K. F.; Hawrylik, S. J.; Lee, S. E.; Scheld, K. G.; Hobart, P. M. X-ray analysis of HIV-1 proteinase at 2.7 A resolution confirms structural homology among retroviral enzymes. *Nature* **1989**, *342*, 299−302.

(13) Navia, M. A.; Fitzgerald, P. M.; McKeever, B. M.; Leu, C. T.; Heimbach, J. C.; Herber, W. K.; Sigal, I. S.; Darke, P. L.; Springer, J. P. Three-dimensional structure of aspartyl protease from human immunodeficiency virus HIV-1. *Nature* **1989**, *337* (6208), 615−620.

(14) Martin, P.; Vickrey, J. F.; Proteasa, G.; Jimenez, Y. L.; Wawrzak, Z.; Winters, M. A.; Merigan, T. C.; Kovari, L. C. "Wide-open" 1.3 A structure of a multidrug-resistant HIV-1 protease as a drug target. *Structure* **2005**, *13* (12), 1887−1895.

(15) Layten, M.; Hornak, V.; Simmerling, C. The open structure of a multi-drug-resistant HIV-1 protease is stabilized by crystal packing contacts. *J. Am. Chem. Soc.* **2006**, *128* (41), 13360−13361.

(16) Hornak, V.; Okur, A.; Rizzo, R. C.; Simmerling, C. HIV-1 protease flaps spontaneously close to the correct structure in simulations following manual placement of an inhibitor into the open state. *J. Am. Chem. Soc.* **2006**, *128* (9), 2812−2813.

(17) Toth, G.; Borics, A. Closing of the flaps of HIV-1 protease induced by substrate binding: a model of a flap closing mechanism in retroviral aspartic proteases. *Biochemistry* **2006**, *45* (21), 6606−6614.

(18) Chang, C. E.; Trylska, J.; Tozzini, V.; McCammon, J. A. Binding pathways of ligands to HIV-1 protease: coarse-grained and atomistic simulations. *Chem. Biol. Drug Des.* **2007**, *69* (1), 5−13.

(19) Zoete, V.; Michielin, O.; Karplus, M. Relation between sequence and structure of HIV-1 protease inhibitor complexes: a model system for the analysis of protein flexibility. *J. Mol. Biol.* **2002**, *315* (1), 21−52.

(20) Ghosh, A. K. *Aspartic Acid Proteases as Therapeutic Targets*; John Wiley and Sons: 2011.

(21) De Meyer, S.; Azijn, H.; Surleraux, D.; Jochmans, D.; Tahri, A.; Pauwels, R.; Wigerinck, P.; de Bethune, M. P. TMC114, a novel human immunodeficiency virus type 1 protease inhibitor active against protease inhibitor-resistant viruses, including a broad range of clinical isolates. *Antimicrob. Agents Chemother.* **2005**, *49* (6), 2314−2321.

(22) Kovalevsky, A. Y.; Liu, F.; Leshchenko, S.; Ghosh, A. K.; Louis, J. M.; Harrison, R. W.; Weber, I. T. Ultra-high resolution crystal structure of HIV-1 protease mutant reveals two binding sites for clinical inhibitor TMC114. *J. Mol. Biol.* **2006**, *363*, 161−173.

(23) Ghosh, A. K.; Anderson, D. D.; Weber, I. T.; Mittsuya, H. Enhancing Protein Backbone Binding-A Fruitful Concept for Combating Drug-Resistant HIV. *Angew. Chem., Int. Ed.* **2012**, *51*, 1778−1802.

(24) Kovalevsky, A. Y.; Tie, Y.; Liu, F.; Boross, P. I.; Wang, Y. F.; Leshchenko, S.; Ghosh, A. K.; Harrison, R. W.; Weber, I. T. Effectiveness of nonpeptide clinical inhibitor TMC-114 on HIV-1 protease with highly drug resistant mutations D30N, I50V, and L90M. *J. Med. Chem.* **2006**, *49* (4), 1379−1387.

(25) Bakry, R.; Vallant, R. M.; Najam-ul-Haq, M.; Rainer, M.; Szabo, Z.; Huck, C. W.; Bonn, G. K. Medicinal applications of fullerenes. *Int. J. Nanomed.* **2007**, *2* (4), 639−649.

(26) Bosi, S.; Da Ros, T.; Spalluto, G.; Prato, M. Fullerene derivatives: an attractive tool for biological applications. *Eur. J. Med. Chem.* **2003**, *38* (11−12), 913−923.
(27) Calvaresi, M.; Zerbetto, F. Baiting proteins with C60. *ACS Nano* **2010**, *4* (4), 2283−2299.
(28) Sivaraman, N.; Srinivasan, T. G.; Vasudeva Rao, P. R.; Natarajan, R. QSPR modeling for solubility of fullerene (C(60)) in organic solvents. *J. Chem. Inf. Comput. Sci.* **2001**, *41* (4), 1067−1074.
(29) Friedman, S. H.; DeCamp, D. L.; Sijbesma, R. P.; Srdanov, G.; Wudl, F.; Kenyon, G. L. Inhibition of the HIV- 1 Protease by Fullerene Derivatives: Model Building Studies and Experimental Verification. *J. Am. Chem. Soc.* **1993**, *115*, 6506−6509.
(30) Sijbesma, R.; Srdanov, G.; Wudl, F.; Castoro, J. A.; Wilkins, C.; Friedman, S. H.; DeCamp, D. L.; Kenyon, G. L. Synthesis of a fullerene derivative for the inhibition of HIV enzymes. *J. Am. Chem. Soc.* **1993**, *115* (15), 6510−6512.
(31) Yin, J.; Nigh, M.; Vanderveer, D.; Jiang, Y.; Wang, X.; Chen, F. Unexpected formation of N-methylfulleropyrrolidines by the reaction of fullerene and gossypol and their bioactivity. *Carbon* **2009**, *47* (12), 2883−2888.
(32) Wlodawer, A.; Vondrasek, J. Inhibitors of HIV-1 protease: a major success of structure-assisted drug design. *Annu. Rev. Biophys. Biomol. Struct.* **1998**, *27*, 249−284.
(33) Back, D.; Sekar, V.; Hoetelmans, R. M. Darunavir: pharmacokinetics and drug interactions. *Antiviral Ther.* **2008**, *13* (1), 1−13.
(34) Case, D. A.; Cheatham, T. E., III; Darden, T.; Gohlke, H.; Luo, R.; Merz, K. M., Jr.; Onufriev, A.; Simmerling, C.; Wang, B.; Woods, R. J. The Amber biomolecular simulation programs. *J. Comput. Chem.* **2005**, *26* (16), 1668−1688.
(35) Case, D. A.; Darden, T. A.; Cheatham, T. E., III; Simmerling, C. L.; Wang, J.; Duke, R. E.; Luo, R.; Walker, R. C.; Zhang, W.; Merz, K. M.; Roberts, B. P.; Wang, B.; Hayik, S.; Roitberg, A.; Seabra, G.; Kolossvai, I.; Wong, K. F.; Paesani, F.; Vanicek, J.; Liu, J.; Wu, X.; Brozell, S. R.; Steinbrecher, T.; Gohlke, H.; Cai, Q.; Ye, X.; Wang, J.; Hsieh, M.-J.; Cui, G.; Roe, D. R.; Mathews, D. H.; Seetin, M. G.; Sagui, C.; Babin, V.; Luchko, T.; Gusarov, S.; Kovalenko, A.; Kollman, P. A. *AMBER 11*; University of California, San Francisco, 2010.
(36) Frisch, M. J.; Trucks, G. W.; Schlegel, H. B.; Scuseria, G. E.; Robb, M. A.; Cheeseman, J. R.; Scalmani, G.; Barone, V.; Mennucci, B.; Petersson, G. A.; Nakatsuji, H.; Caricato, M.; Li, X.; Hratchian, H. P.; Izmaylov, A. F.; Bloino, J.; Zheng, G.; Sonnenberg, J. L.; Hada, M.; Ehara, M.; Toyota, K.; Fukuda, R.; Hasegawa, J.; Ishida, M.; Nakajima, T.; Honda, Y.; Kitao, O.; Nakai, H.; Vreven, T.; Montgomery, Jr., J. A.; Peralta, J. E.; Ogliaro, F.; Bearpark, M.; Heyd, J. J.; Brothers, E.; Kudin, K. N.; Staroverov, V. N.; Kobayashi, R.; Normand, J.; Raghavachari, K.; Rendell, A.; Burant, J. C.; Iyengar, S. S.; Tomasi, J.; Cossi, M.; Rega, N.; Millam, N. J.; Klene, M.; Knox, J. E.; Cross, J. B.; Bakken, V.; Adamo, C.; Jaramillo, J.; Gomperts, R.; Stratmann, R. E.; Yazyev, O.; Austin, A. J.; Cammi, R.; Pomelli, C.; Ochterski, J. W.; Martin, R. L.; Morokuma, K.; Zakrzewski, V. G.; Voth, G. A.; Salvador, P.; Dannenberg, J. J.; Dapprich, S.; Daniels, A. D.; Farkas, Ö.; Foresman, J. B.; Ortiz, J. V.; Cioslowski, J.; Fox, D. J. *Gaussian 09*; Gaussian, Inc.: Wallingford, CT, 2009.
(37) Wang, J.; Wolf, R. M.; Caldwell, J. W.; Kollman, P. A.; Case, D. A. Development and testing of a general amber force field. *J. Comput. Chem.* **2004**, *25* (9), 1157−1174.
(38) Woods, R. J.; Khalil, M.; Pell, W.; Moffat, S. H.; Smith, V. H. Derivation of Net Atomic Charges from Molecular Electrostatic Potentials. *J. Comput. Chem.* **1990**, *11* (3), 297−310.
(39) Jorgensen, W. L.; Chandrasekhar, J.; Madura, J. D.; Impey, R. W.; Klein, M. L. Comparison of simple potential functions for simulating liquid water. *J. Chem. Phys.* **1983**, *79*, 926−935.
(40) Ryckaert, J. P.; Ciccotti, G.; Berendsen, H. J. C. Numerical Integration of the Cartesian Equations of Motion of a System with Constraints: Molecular Dynamics of n-Alkanes. *J. Comput. Phys.* **1977**, *23*, 327−341.
(41) Izaguirre, J. A.; Catarello, D. P.; Wozniak, J. M.; Skeel, R. D. Langevin Stabilization of Molecular Dynamics. *J. Chem. Phys.* **2001**, *114* (4), 2090−2098.
(42) Hyland, L. J.; Tomaszek, T. A., Jr.; Meek, T. D. Human immunodeficiency virus-1 protease. 2. Use of pH rate studies and solvent kinetic isotope effects to elucidate details of chemical mechanism. *Biochemistry* **1991**, *30* (34), 8454−8463.
(43) Pietrucci, F.; Marinelli, F.; Carloni, P.; Laio, A. Substrate binding mechanism of HIV-1 protease from explicit-solvent atomistic simulations. *J. Am. Chem. Soc.* **2009**, *131* (33), 11811−11818.
(44) Hou, T.; McLaughlin, W. A.; Wang, W. Evaluating the potency of HIV-1 protease drugs to combat resistance. *Proteins* **2008**, *71* (3), 1163−1174.
(45) Hornak, V.; Abel, R.; Okur, A.; Strockbine, B.; Roitberg, A.; Simmerling, C. Comparison of multiple Amber force fields and development of improved protein backbone parameters. *Proteins* **2006**, *65* (3), 712−725.
(46) Darden, T.; York, D.; Pedersen, L. Particle Mesh Ewald-an N.Log(N) method for Ewald sums in large systems. *J. Chem. Phys.* **1993**, *98*, 10089−10092.
(47) Hawkins, G. D.; Cramer, C. J.; Truhlar, D. G. Parametrized Models of Aqueous Free Energies of Solvation Based on Pairwise Descreening of Solute Atomic Charges from a Dielectric Medium. *J. Phys. Chem.* **1996**, *100* (51), 19824−19839.
(48) Schuttelkopf, A. W.; van Aalten, D. M. PRODRG: a tool for high-throughput crystallography of protein-ligand complexes. *Acta Crystallogr., Sect. D: Biol. Crystallogr.* **2004**, *60* (Pt 8), 1355−1363.
(49) Berger, O.; Edholm, O.; Jahnig, F. Molecular dynamics simulations of a fluid bilayer of dipalmitoylphosphatidylcholine at full hydration, constant pressure, and constant temperature. *Biophys. J.* **1997**, *72* (5), 2002−2013.
(50) Tieleman, D. P.; Berendsen, H. J. Molecular dynamics simulations of a fully hydrated dipalmitoylphosphatidylcholine bilayer with different macroscopic boundary conditions and parameters. *J. Chem. Phys.* **1996**, *105*, 4871−4880.
(51) Berendsen, H. J. C.; Postma, J. P. M.; van Gunsteren, W. F.; Hermans, J. Interaction models for water in relation to protein hydration. *Intermol. Forces* **1981**, *11*, 331−338.
(52) Berendsen, H. J. C.; van der Spoel, D.; van Drunen, R. GROMACS: A message-passing parallel molecular dynamics implementation. *Comput. Phys. Commun.* **1995**, *91*, 43−56.
(53) Hess, B.; Kutzner, C.; van der Spoel, D.; Lindhal, E. GROMACS 4: Algorithms for Highly Efficient, Load-Balanced, and Scalable Molecular Simulation. *J. Chem. Theory Comput.* **2008**, *4*, 435−447.
(54) Van der Spoel, D.; Lindahl, E.; Hess, B.; Groenhof, G.; Mark, A. E.; Berendsen, H. J. GROMACS: fast, flexible, and free. *J. Comput. Chem.* **2005**, *26* (16), 1701−1718.
(55) Van der Spoel, D.; Lindahl, E.; Hess, B.; van Buuren, A. R.; Apol, E.; Meulenhoff, P. J.; Sijbers, A.; Feenstra, K. A.; van Drumen, R.; Berendsen, H. J. C. *GROMACS User Manual*, version 4.5; Nijenborgh 4, 2010.
(56) Hess, B.; Bekker, H.; Berendsen, H. J. C.; Fraaije, J. G. E. M. LINCS: A linear constraint solver for molecular simulations. *J. Comput. Chem.* **1997**, *18*, 1463−1472.
(57) Berendsen, H. J. C.; Postma, J. P. M. D. A.; Haak, J. R. Molecular dynamics with coupling to an external bath. *J. Chem. Phys.* **1984**, *81*, 3684−3690.
(58) Thompson, M. A. *ArgusLab 4.0.1*; Planaria Software LLC: Seattle, WA.
(59) Simmerling, C.; Elber, R.; Zhang, J. Moil-view—A program for visualization of structure and dynamics of biomolecules and STO—A program for computing stochastic paths. In *Modeling of Biomolecular Structures and Mechanisms*; Pullman, A. et al., Eds.; Kluwer Acad. Publishers: Netherlands, 1995.
(60) Pettersen, E. F.; Goddard, T. D.; Huang, C. C.; Couch, G. S.; Greenblatt, D. M.; Meng, E. C.; Ferrin, T. E. UCSF Chimera--a visualization system for exploratory research and analysis. *J. Comput. Chem.* **2004**, *25* (13), 1605−1612.

(61) Jorgensen, W. L. The many roles of computation in drug discovery. *Science* **2004**, *303* (5665), 1813−1818.
(62) Wang, W.; Donini, O.; Reyes, C. M.; Kollman, P. A. Biomolecular simulations: recent developments in force fields, simulations of enzyme catalysis, protein-ligand, protein-protein, and protein-nucleic acid noncovalent interactions. *Annu. Rev. Biophys. Biomol. Struct.* **2001**, *30*, 211−243.
(63) Bash, P. A.; Singh, U. C.; Brown, F. K.; Langridge, R.; Kollman, P. A. Calculation of the relative change in binding free energy of a protein-inhibitor complex. *Science* **1987**, *235* (4788), 574−576.
(64) Gao, J.; Kuczera, K.; Tidor, B.; Karplus, M. Hidden thermodynamics of mutant proteins: a molecular dynamics analysis. *Science* **1989**, *244* (4908), 1069−1072.
(65) Lawrenz, M.; Baron, R.; McCammon, J. A. Independent-Trajectories Thermodynamic-Integration Free-Energy Changes for Biomolecular Systems: Determinants of H5N1 Avian Influenza Virus Neuraminidase Inhibition by Peramivir. *J. Chem. Theory Comput.* **2009**, *5* (4), 1106−1116.
(66) Aqvist, J.; Medina, C.; Samuelsson, J. E. A new method for predicting binding affinity in computer-aided drug design. *Protein Eng.* **1994**, *7* (3), 385−391.
(67) Perdih, A.; Bren, U.; Solmajer, T. Binding free energy calculations of N-sulphonyl-glutamic acid inhibitors of MurD ligase. *J. Mol. Model.* **2009**, *15* (8), 983−996.
(68) Bren, U.; Martinek, V.; Florian, J. Free energy simulations of uncatalyzed DNA replication fidelity: structure and stability of T.G and dTTP.G terminal DNA mismatches flanked by a single dangling nucleotide. *J. Phys. Chem. B* **2006**, *110* (21), 10557−10566.
(69) Lee, F. S.; Chu, Z. T.; Bolger, M. B.; Warshel, A. Calculations of antibody-antigen interactions: microscopic and semi-microscopic evaluation of the free energies of binding of phosphorylcholine analogs to McPC603. *Protein Eng.* **1992**, *5* (3), 215−228.
(70) Carlsson, J.; Boukharta, L.; Aqvist, J. Combining docking, molecular dynamics and the linear interaction energy method to predict binding modes and affinities for non-nucleoside inhibitors to HIV-1 reverse transcriptase. *J. Med. Chem.* **2008**, *51*, 2648−2656.
(71) Smith, R. H., Jr.; Jorgensen, W. L.; Tirado-Rives, J.; Lamb, M. L.; Janssen, P. A.; Michejda, C. J.; Kroeger Smith, M. B. Prediction of binding affinities for TIBO inhibitors of HIV-1 reverse transcriptase using Monte Carlo simulations in a linear response method. *J. Med. Chem.* **1998**, *41* (26), 5272−5286.
(72) Bren, U.; Lah, J.; Bren, M.; Martinek, V.; Florian, J. DNA duplex stability: the role of preorganized electrostatics. *J. Phys. Chem. B* **2010**, *114* (8), 2876−2885.
(73) Gohlke, H.; Kiel, C.; Case, D. A. Insights into protein-protein binding by binding free energy calculation and free energy decomposition for the Ras-Raf and Ras-RalGDS complexes. *J. Mol. Biol.* **2003**, *330* (4), 891−913.
(74) Wang, W.; Kollman, P. A. Computational study of protein specificity: the molecular basis of HIV-1 protease drug resistance. *Proc. Natl. Acad. Sci. U. S. A.* **2001**, *98* (26), 14937−14942.
(75) Xu, Y.; Wang, R. A computational analysis of the binding affinities of FKBP12 inhibitors using the MM-PB/SA method. *Proteins* **2006**, *64* (4), 1058−1068.
(76) Kollman, P. A.; Massova, I.; Reyes, C.; Kuhn, B.; Huo, S.; Chong, L.; Lee, M.; Lee, T.; Duan, Y.; Wang, W.; Donini, O.; Cieplak, P.; Srinivasan, J.; Case, D. A.; Cheatham, T. E., III Calculating structures and free energies of complex molecules: combining molecular mechanics and continuum models. *Acc. Chem. Res.* **2000**, *33* (12), 889−897.
(77) Honig, B.; Nicholls, A. Classical electrostatics in biology and chemistry. *Science* **1995**, *268* (5214), 1144−1149.
(78) Stoica, I.; Sadiq, S. K.; Coveney, P. V. Rapid and accurate prediction of binding free energies for saquinavir-bound HIV-1 proteases. *J. Am. Chem. Soc.* **2008**, *130* (8), 2639−2648.
(79) Weiser, J.; Shenkin, P. S.; Still, W. C. Approximate atomic surfaces from linear combinations of pairwise overlaps (LCPO). *J. Comput. Chem.* **1999**, *20*, 217−230.
(80) Bren, U.; Martinek, V.; Florian, J. Decomposition of the solvation free energies of deoxyribonucleoside triphosphates using the free energy perturbation method. *J. Phys. Chem. B* **2006**, *110* (25), 12782−12788.
(81) Bren, M.; Florian, J.; Mavri, J.; Bren, U. Do all pieces make a whole? Thiele cumulants and the free energy decomposition. *Theor. Chem. Acc.* **2007**, *117*, 535−540.
(82) Shrake, A.; Rupley, J. A. Environment and exposure to solvent of protein atoms. Lysozyme and insulin. *J. Mol. Biol.* **1973**, *79* (2), 351−371.
(83) Sokalski, W. A.; Roszak, S. M. Efficient techniques for the decomposition of intermolecular interaction energy at SCF level and beyond. *J. Mol. Struct. (Theochem)* **1991**, *234*, 387−400.
(84) Sokalski, W. A.; Roszak, S.; Pecul, K. An efficient procedure for decomposition of the SCF interaction energy into components with reduced basis set dependence. *Chem. Phys. Lett.* **1988**, *153*, 153−159.
(85) Gora, R. W.; Grabowski, S. J.; Leszczynski, J. Dimers of formic acid, acetic acid, formamide and pyrrole-2-carboxylic acid: an ab initio study. *J. Phys. Chem. A* **2005**, *109* (29), 6397−6405.
(86) Gora, R. W.; Sokalski, W. A.; Leszczynski, J.; Pett, V. B. The nature of interactions in the ionic crystal of 3-pentenenitrile, 2-nitro-5-oxo, ion(−1), sodium. *J. Phys. Chem. B* **2005**, *109* (5), 2027−2033.
(87) Gora, R. W.; Bartkowiak, W.; Roszak, S.; Leszczynski, J. Intermolecular interactions in solution: Elucidating the influence of the solvent. *J. Chem. Phys.* **2004**, *120*, 2802−2813.
(88) Gora, W.; Bartkowiak, W.; Roszak, S.; Leszczynski, J. A new theoretical insight into the nature of intermolecular interactions in the molecular crystal of urea. *J. Chem. Phys.* **2002**, *117*, 1031−1039.
(89) Gora, R. W. EDS package, Revision 2.8.1; Wrocław, Poland, 1998−2008.
(90) Schmidt, M. W.; Baldridge, K. K.; Boatz, J. A.; Elbert, S. T.; Gordon, M. S.; Jensen, J. H.; Koseki, S.; Matsunaga, N.; Nguyen, K. A.; Su, S.; Windus, T. L.; Dupuis, M.; Montgomery, J. A. General atomic and molecular electronic structure system. *J. Comput. Chem.* **1993**, *14*, 1347−1363.
(91) Czyznikowska, Z. How does modification of adenine by hydroxyl radical influence the stability and the nature of stacking interactions in adenine-cytosine complex? *J. Mol. Model.* **2009**, *15* (6), 615−622.
(92) Czyznikowska, Z.; Gora, R. W.; Zalesny, R.; Lipkowski, P.; Jarzembska, K. N.; Dominiak, P. M.; Leszczynski, J. Structural variability and the nature of intermolecular interactions in Watson-Crick B-DNA base pairs. *J. Phys. Chem. B* **2010**, *114*, 9629−9644.
(93) Czyznikowska, Z.; Lipkowski, P.; Gora, R. W.; Zalesny, R.; Cheng, A. C. On the nature of intermolecular interactions in nucleic acid base-amino acid side-chain complexes. *J. Phys. Chem. B* **2009**, *113* (33), 11511−11520.
(94) Gora, R. W.; Roszak, S.; Leszczynski, J. The molecular structures and nature of interactions in $CH_3^+Ar_n$ (n = 1−8) complexes. *J. Chem. Phys.* **2001**, *115*, 771−777.
(95) Cybulski, S. M.; Chalasinski, G.; Moszyński, R. On decomposition of second−order Møller−Plesset supermolecular interaction energy and basis set effects. *J. Chem. Phys.* **1990**, *92*, 4357−4363.
(96) Gustchina, A.; Sansom, C.; Prevost, M.; Richelle, J.; Wodak, S. Y.; Wlodawer, A.; Weber, I. T. Energy calculations and analysis of HIV-1 protease-inhibitor crystal structures. *Protein Eng.* **1994**, *7* (3), 309−317.
(97) Todd, M. J.; Luque, I.; Velazquez-Campoy, A.; Freire, E. Thermodynamic basis of resistance to HIV-1 protease inhibition: calorimetric analysis of the V82F/I84V active site resistant mutant. *Biochemistry* **2000**, *39* (39), 11876−11883.
(98) Waters, L.; Nelson, M. Why do patients fail HIV therapy? *Int. J. Clin. Pract.* **2007**, *61* (6), 983−990.
(99) Ghosh, A. K.; Ramu Sridhar, P.; Kumaragurubaran, N.; Koh, Y.; Weber, I. T.; Mitsuya, H. Bis-tetrahydrofuran: a privileged ligand for darunavir and a new generation of hiv protease inhibitors that combat drug resistance. *ChemMedChem* **2006**, *1*, 939−950.

(100) Sham, H. L.; Kempf, D. J.; Molla, A.; Marsh, K. C.; Kumar, G. N.; Chen, C. M.; Kati, W.; Stewart, K.; Lal, R.; Hsu, A.; Betebenner, D.; Korneyeva, M.; Vasavanonda, S.; McDonald, E.; Saldivar, A.; Wideburg, N.; Chen, X.; Niu, P.; Park, C.; Jayanti, V.; Grabowski, B.; Granneman, G. R.; Sun, E.; Japour, A. J.; Leonard, J. M.; Plattner, J. J.; Norbeck, D. W. ABT-378, a highly potent inhibitor of the human immunodeficiency virus protease. *Antimicrob. Agents Chemother.* **1998**, *42* (12), 3218−3224.
(101) Muzammil, S.; Armstrong, A. A.; Kang, L. W.; Jakalian, A.; Bonneau, P. R.; Schmelmer, V.; Amzel, L. M.; Freire, E. Unique thermodynamic response of tipranavir to human immunodeficiency virus type 1 protease drug resistance mutations. *J. Virol.* **2007**, *81* (10), 5144−5154.
(102) Shurtleff, A. C. TMC-114 (Tibotec). *Curr. Opin. Invest. Drugs (BioMed Cent.)* **2004**, *5*, 879−886.
(103) Johnson, V. A.; Brun-Vezinet, F.; Clotet, B.; Gunthard, H. F.; Kuritzkes, D. R.; Pillay, D.; Schapiro, J. M.; Richman, D. D. Update of the Drug Resistance Mutations in HIV-1. *Top. HIV Med.* **2008**, *16* (5), 138−145.
(104) Wolfe, C.; Hicks, C. Profile of darunavir in the management of treatment-experienced HIV patients. *HIV AIDS (Auckland)* **2009**, *1*, 13−21.
(105) Koh, Y.; Matsumi, S.; Das, D.; Amano, M.; Davis, D. A.; Li, J.; Leschenko, S.; Baldridge, A.; Shioda, T.; Yarchoan, R.; Ghosh, A. K.; Mitsuya, H. Potent inhibition of HIV-1 replication by novel non-peptidyl small molecule inhibitors of protease dimerization. *J. Biol. Chem.* **2007**, *282* (39), 28709−28720.
(106) Liu, F.; Boross, P. I.; Wang, Y. F.; Tozser, J.; Louis, J. M.; Harrison, R. W.; Weber, I. T. Kinetic, stability, and structural changes in high-resolution crystal structures of HIV-1 protease with drug-resistant mutations L24I, I50V, and G73S. *J. Mol. Biol.* **2005**, *354* (4), 789−800.
(107) Liu, F.; Kovalevsky, A. Y.; Louis, J. M.; Boross, P. I.; Wang, Y. F.; Harrison, R. W.; Weber, I. T. Mechanism of drug resistance revealed by the crystal structure of the unliganded HIV-1 protease with F53L mutation. *J. Mol. Biol.* **2006**, *358* (5), 1191−1199.
(108) Kovalevsky, A. Y.; Chumanevich, A. A.; Liu, F.; Louis, J. M.; Weber, I. T. Caught in the Act: the 1.5 A resolution crystal structures of the HIV-1 protease and the I54V mutant reveal a tetrahedral reaction intermediate. *Biochemistry* **2007**, *46* (51), 14854−14864.
(109) Friedman, S. H.; Ganapathi, P. S.; Rubin, Y.; Kenyon, G. L. Optimizing the Binding of Fullerene Inhibitors of the HIV-1 Protease through Predicted Increases in Hydrophobic Desolvation. *J. Med. Chem.* **1998**, *41* (13), 2424−2429.
(110) Toczyłowski, R. R.; Cybulski, S. M. An Analysis of the Interactions between Nucleic Acid Bases: Hydrogen−Bonded Base Pairs. *J. Phys. Chem. A* **2003**, *107*, 418−426.
(111) Costigan, S. C.; Booth, P. J.; Templer, R. H. Estimations of lipid bilayer geometry in fluid lamellar phases. *Biochim. Biophys. Acta* **2000**, *1468* (1−2), 41−54.
(112) Hogberg, C. J.; Lyubartsev, A. P. A molecular dynamics investigation of the influence of hydration and temperature on structural and dynamical properties of a dimyristoylphosphatidylcholine bilayer. *J. Phys. Chem. B* **2006**, *110* (29), 14326−14336.
(113) Mojumdar, E. H.; Lyubartsev, A. P. Molecular dynamics simulations of local anesthetic articaine in a lipid bilayer. *Biophys. Chem.* **2010**, *153* (1), 27−35.
(114) Nagle, J. F.; Tristram-Nagle, S. Structure of lipid bilayers. *Biochim. Biophys. Acta* **2000**, *1469* (3), 159−195.
(115) Petrache, H. I.; Dodd, S. W.; Brown, M. F. Area per lipid and acyl length distributions in fluid phosphatidylcholines determined by (2)H NMR spectroscopy. *Biophys. J.* **2000**, *79* (6), 3172−3192.